A Doctoral Dissertation

Dynamics of Multicomponent Polymer Systems

(多成分系高分子のダイナミクス)

Takayuki Ikehara

(池原 飛之)

Preface

The scientific investigations of the dynamics of multicomponent polymer systems are becoming more important since practical polymeric materials often contain multicomponents. This thesis focuses on dynamics of polymeric gels (part I), the crystallization in multicomponent polymer systems (part II), and miscible polymer blends (part III), and discuss the dynamics of these systems.

Part I consists of two topics. One is the change of the volume of the gels in polymeric solutions (chapter 1). The volume of acrylamide gel in aqueous solution of poly(vinyl methyl ether) (PVME) was studied. The gel, which was originally at the equilibrium swelling state in distilled water, contracted when transferred into the solution because of the osmotic pressure difference between the inside and outside of the gel. Moreover, it began to swell again after that. The kinetics of the initial collapse was governed by the cooperative diffusion equation. The shrinking stopped when the osmotic pressure of the gel was equal to that of the solution. The volume at this moment decreased with the concentration of the solution. The rate of the re-swelling after the initial collapse depended on the concentration of the solution. These phenomena were explained in terms of penetration of PVME molecules into the network.

The other is the investigation of acrylamide gels from the view point of molecular mobility (chapter 2). Both ionized and non-ionized acrylamide gels in acetone-water mixture were studied by pulsed NMR. We investigated (i) dependence of the spin-spin relaxation time T_2 of the gels on the composition of the solvent, (ii) temporal changes of T_2 during the volume phase transition process for the ionized gels, and (iii) domain sizes of heterogeneous structures in the non-ionized gels caused by abrupt changes of the environment using the spin diffusion phenomenon. The results of the concentration dependence of T_2 showed that molecular mobility of both the solvent and the network was further depressed as the acetone content was increased in the contracted state although the volume change was small. These results show that the interaction parameter between the solvent and the network polymer has more influence on the mobility than the volume of the system. The shrinking and the swelling process of gels undergoing volume phase transition were different from each other. This reflects the behavior that the swelling and shrinking start on the boundary of the samples. The obtained domain sizes of the heterogeneous structure indicate that solid-like regions are formed on a smaller scale in the dense phase of the network.

Part II also consists of two topics. One is the crystallization process of crystalline/amorphous polymer blends (chapter 3). The crystallization process of poly(ϵ-caprolactone)/oligostyrene (PCL/OS) blends was analyzed by measuring the spin-spin relaxation time T_2 by pulsed NMR. We examined (i) the temporal changes of T_2 and the

fractional amount f of the crystalline, amorphous, and intermediate components in the primary and secondary crystallization processes and (ii) the dependence of the behavior on the crystallization temperature T_c and the OS content ϕ_{OS}. The decrease of T_2 of the intermediate and amorphous components with increasing ϕ_{OS} indicated that OS rejected during crystallization is mixed with the residual amorphous PCL as well as trapped in the interface between a lamellar crystal and an amorphous layer. The fraction of the crystal, which is the crystallinity based on the number of protons, decreased with increasing T_c. This is ascribed to the polydispersity of PCL. The values of f of the crystalline and amorphous components depended less on T_c and ϕ_{OS} after the secondary crystallization proceeded than at the end of the primary process. This indicates that the secondary crystallization has the effect of annealing. The fraction of the interface can be an index of regularity of the lamellar structure. Its change implied which process of lamellar thickening, lamella generation, and the rejection of OS was dominant in the secondary crystallization. We also discussed which region OS was rejected into. The changes of f of the three components in the secondary process showed extreme values at $\phi_{OS} \simeq 5\%$. To discuss this behavior, we proposed two possibilities, i. e. the influence of the morphology of the spherulites and local phase separation during crystallization.

The other topic is the investigation of morphology of crystalline/crystalline polymer blends by optical microscopy (chapter 4). Interpenetrated spherulites of poly(butylene succinate)/poly (vinylidene chloride-*co*-vinyl chloride) (PBSU/PVDCVC) blends were investigated by optical microscopy. The spherulites of PBSU and PVDCVC were negative and positive respectively, and birefringence of PVDCVC was small under crossed nicols. The spherulitic growth rate of PVDCVC showed complex dependence on the crystallization temperature T_c. Interpenetrated spherulites were formed under most of the experimental conditions, PBSU content 30%–60% and T_c 338 K–378 K. Optical microscopy revealed that the birefringent pattern of the area of a PVDCVC spherulite changed into that of a PBSU spherulite after penetration. This result indicates that the lamellae of PBSU grow along those of PVDCVC, and it is the evidence for the formation of interpenetrated spherulites. The microscopic observations implied that the density of lamellae in PVDCVC was sparse. The birefringent pattern of PBSU spherulites changed with experimental conditions. The blends with low PBSU content showed neither negative nor positive spherulite. This birefringence was also kept in the area of PVDCVC spherulites after penetration.

Finally in part III, dynamics of miscible polymer blends was investigated in terms of molecular mobility (chapter 5). The spin-lattice relaxation time T_1 and that in the rotating frame $T_{1\rho}$ of polystyrene/poly(vinyl methyl ether) (PS/PVME) blends showed a single decaying component in the miscible state. The spin-spin relaxation, on the other hand, showed two relaxing components, and the relaxation time T_2 changed continuously with the PS content ϕ. The fractional amounts of the two components coincided with the fraction of the protons in the two constituent polymers calculated from ϕ. These results were discussed based on two models: (i) microscopic phase separation even in the miscible state and (ii) the difference in molecular mobility between the two polymers mixed on the molecular level. The latter assumption explained the experimental results better.

Bibliography

1. T. Ikehara and T. Nishi, "Combined collapse-swelling behavior of acrylamide gel in polymeric solution", Phys. Rev. Lett., **71**, 2497 (1993).

2. T. Ikehara and T. Nishi, "Temporal change of the volume of gels in polymer solution", Trans. Mat. Res. Soc. Jpn., **15A**, 221 (1994).

3. T. Ikehara, T. Nishi and T. Hayashi, "Volume phase transition process and spin diffusion in heterogeneous structure of acrylamide gels studied by pulsed NMR", Polym. J., **28**, 169 (1996).

4. T. Ikehara and T. Nishi, "Pre-ordering state in the crystallization process of polymer blends detected by pulsed NMR", Acta Polym., **46**, 416 (1995).

5. T. Ikehara and T. Nishi, "Primary and secondary crystallization processes of poly(ϵ-caprolactone)/styrene oligomer blends investigated by pulsed NMR", Polymer, **41**, 7855 (2000).

6. T. Ikehara and T. Nishi, "Interpenetrated Spherulites of Poly(butylene succinate)/ poly(vinylidene chloride-*co*-vinyl chloride) Blends. An Optical Microscopic Study", Polym. J., **32**, 683 (2000).

Award

- "Award for the Outstanding Paper" published in Polymer Journal, Society of Polymer Science, Japan (1996).

Contents

Part I

Dynamics of Gels

Chapter 1

Polyacrylamide gels in polymeric solutions

1.1 Introduction

Behavior of volume of polymeric gels has attracted a lot of interest since the discovery of volume phase transition [1]. The volume varies with changing the external environment, such as concentration of mixed solvents [1, 2], temperature [3], pH [4], and salt concentration [5]. There have also been works on gels in polymeric solutions [6–11]. These studies showed that initially swollen networks contract when they are immersed into the solutions. The extent of deswelling increases with the concentration and, hence, the osmotic pressure of the solution. One of the problems of these studies is whether polymer molecules in solutions can permeate into networks. Two principal factors are considered to affect permeability: the Flory-Huggins interaction parameter χ between the network and solute polymer, and the relative dimension of the radius of gyration of polymers R_g to the mesh size of networks ξ. A miscible polymer ($\chi < 0$) can penetrate into gel when $R_g < \xi$ and cannot when $R_g > \xi$. In the case that two polymers are immiscible ($\chi > 0$), a little but effective amount of polymer permeates the gel [9]. When the gel is ionized, translational entropy of component counterions produces additional osmotic pressure; this increases the spatial size of the network and hence enhances the permeability [11].

The changes of the volume of polyacrylamide gels in aqueous solution of poly(vinyl methyl ether) (PVME) are discussed here. We will consider the influence of the concentration of the solution on the behavior, the relation between the osmotic pressure of the solution. The kinetics of the shrinking process is also discussed in terms of cooperative diffusion equation of gels [13]. Investigation to obtain direct evidence of existence of PVME in the network by Fourier transform infrared spectroscopy (FTIR) is also demonstrated.

1.2 Experimental

Acrylamide gels were prepared by free radical polymerization [4] with 0.25 g of acrylamide (main chain), 6.6 mg of N,N'-methylene*bis*acrylamide (cross-linking agent), and 0.2 g of sodium acrylate (ionizable molecules) in 5 mℓ of N_2-saturated distilled water. The gelation took place in capillaries with 0.5 mm inner diameter. Cylindrical samples were obtained

and immersed into large amount of water to remove unreacted substances. PVME was purchased from Polysciences, Inc. This sample seems to have broad molecular weight distribution though we have not specifically analyzed it.

Temporal changes of the diameter of gels, d, were measured with a scale on the eyepiece of an optical microscope. The swelling ratio was calculated as $V/V_0 = (d/d_0)^3$, where V is the volume, V_0 is that at gelation, and d_0 is the inner diameter of capillaries (= 0.5 mm). Cylindrical samples were sliced perpendicularly to the axis into disk-like gels, which were used in all experiments. These gels may not be called strictly disk-like since the ratio of the diameter to the thickness was *ca.* 2.5. All measurements were performed at room temperature. This ensures no phase separation in water-PVME mixture.

1.3 Results

As shown in Fig. 1.1, polyacrylamide gels initially contracted when transferred into aqueous solution of PVME. After several hundreds of hours, it started to swell again with the volume approaching the value of the equilibrium swelling state in pure water.

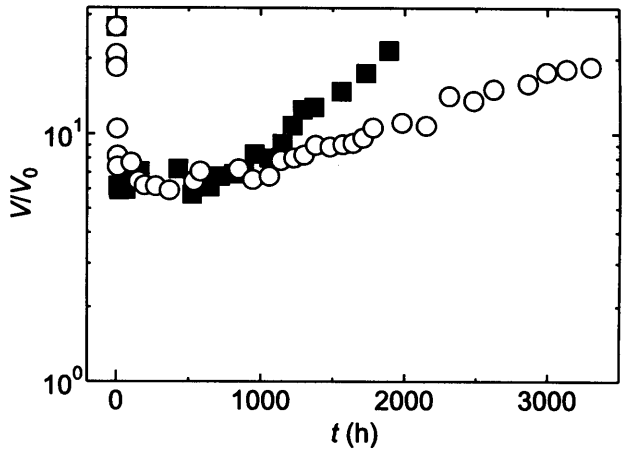

Figure 1.1: Volume change of polyacrylamide gels in aqueous solution of PVME of 0.25 wt.%. The swelling ratio V/V_0, defined as the ratio of the volume to that at gelation, of disk-like (•) and cylindrical gels (□).

Temporal changes of gel volume in PVME solutions of various concentrations are shown in Fig. 1.2. Gels at the equilibrium swelling state in pure water were transferred into PVME solutions at time zero. Gels contracted with the characteristic time shorter than one hour as mentioned in the next section. After that, they began to swell again. This process was slower than the deswelling and depended on the concentration.

The data in Fig. 1.3 provides another evidence to deny the possibility of gels properties changes discussed in [12] and to indicate that PVME penetrates into the network. Before this experiment, the sample had first been re-swollen in solution containing 0.25 wt % PVME. When V/V_0 had increased to *ca.* 8.4 (two months after transferred from pure water), the gel was reimmersed in water to remove PVME from the inside. Because of the higher interior pressure than of the fresh ones, the volume overshot the equilibrium

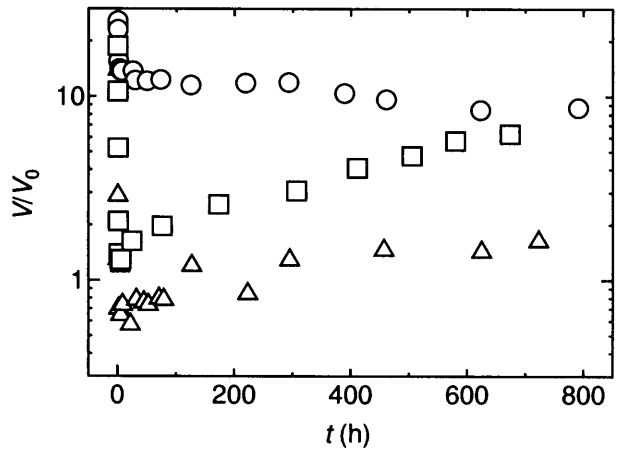

Figure 1.2: Temporal change of swelling ratio of acrylamide gels in aqueous solutions of PVME of various concentrations, 0.1 % (○), 1 % (□), and 5 % (△).

value in pure water, then it gradually approached it downwards. After the sample had been kept there for 16 days, it was transferred again into PVME solution. This moment is the time origin of Fig. 1.3. The gel shows the same change of swelling ratio as shown in Fig. 1.1, except its higher minimum. This is because PVME had not been removed completely from the inside.

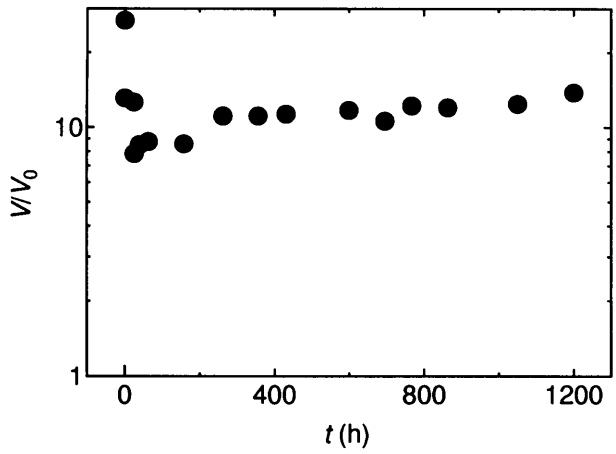

Figure 1.3: Temporal change, in PVME solution of 0.25 wt %, of acrylamide gel which was first re-swollen in the solution, then soaked in pure water for 16 days to remove PVME molecules inside. The sample re-swells analogously.

Figure 1.4 shows FTIR spectra of PVME and a dried polyacrylamide gel that was not soaked in PVME solution. Though many peaks in both spectra appear in close positions, evidence for penetration of PVME can be obtained by examining the peaks at 1082 cm^{-1}, 1379 cm^{-1}, 1186 cm^{-1}, and 2820 cm^{-1}.

Figure 1.5 shows the FTIR spectrum of a dried, reswollen polyacrylamide gel from

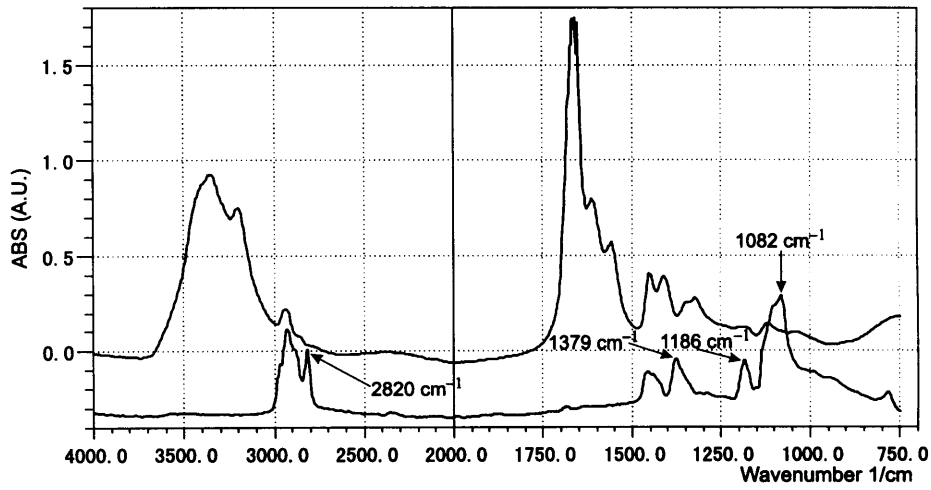

Figure 1.4: FTIR spectra of a dried polyacrylamide gel (top) and PVME (bottom).

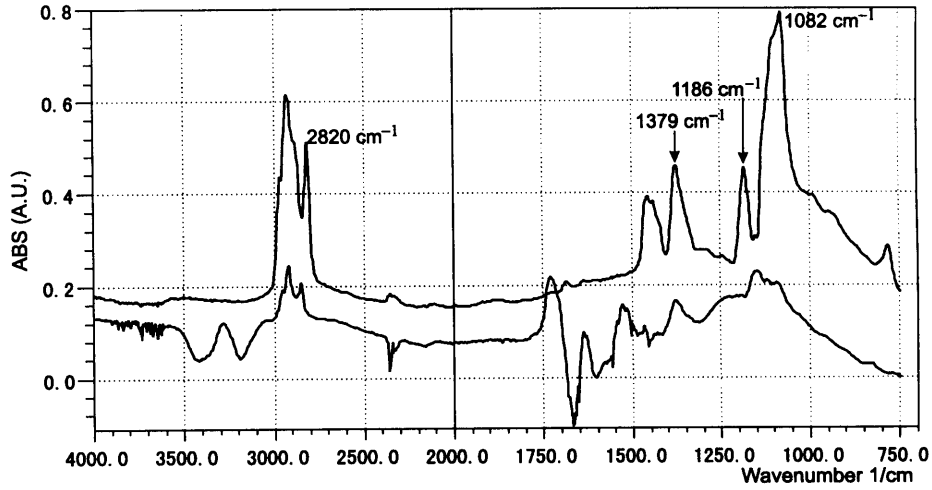

Figure 1.5: The FTIR spectrum of PVME (top) and the spectrum of a reswollen polyacrylamide gel from which that of a dried polyacrylamide was subtracted (bottom).

which that of a non-soaked gel in Fig. 1.4 was subtracted with an appropriate coefficient. The spectrum of PVME is also displayed at the top for comparison. The subtracted spectrum shows the peaks at 1379 cm^{-1} and 2820 cm^{-1} though it does not show distinct peaks at 1082 cm^{-1} and 1186 cm^{-1}.

1.4 Discussions

Figure 1.1 shows a curious phenomenon; in usual non-equilibrium process, when external condition has abruptly been altered, the direction of change of the system is only toward the new equilibrium state under the condition. The process never returns. There were several causes considered to explain the re-swelling, such as the change of properties of PVME solution or acrylamide gel due to oxidation or degradation. Nevertheless, we ascribed the re-swelling to the penetration of PVME molecules into the gel. Thermodynamic analysis can show that it raises the osmotic pressure inside the gel; this leads to the re-swelling.

The initial collapse is a direct result of the difference of osmotic pressure between the inside and outside of gels. They change their volume to sustain the external pressure. The deswelling stops when the internal osmotic pressure equals that of solution. The cooperative diffusion equation governs the kinetics of this type of volume change [13]. According to this theory, the displacement of the size of spherical gels from the ultimate value, $\Delta a(t)$, is expressed, after higher-order terms have decayed, as:

$$\Delta a/\Delta a_0 \sim (6/\pi^2)\exp(-t/\tau). \tag{1.1}$$

where Δa_0 is the total change of the size, a is the ultimate radius of the gel, and the time constant:

$$\tau = a^2/(\pi^2 D), \tag{1.2}$$

where D is the cooperative diffusion coefficient of the network. Figure 1.6 shows the semi-log plot of the temporal change of $\Delta a/\Delta a_0$ in 1 % solution. It should be noted that the kinetics of thick disk-like gels whose diameter and length are of the same order is governed by the same equation as spherical ones [14]. The deviation from the line in the early stage in Fig. 1.6 represents the higher order terms of Eq. 1.1. The value of τ was obtained from the slope as 1.7×10^3 s. We obtained almost the same value for characteristic times at other concentrations. With τ and Eq. 1.2, one can calculate the value of D as 3.5×10^{-7} cm^2/s. This value agrees well with ones obtained by other authors (2.9–4.1×10^{-7} cm^2/s) [13–15].

Figure 1.2 shows the concentration dependence of re-swelling behavior, which is caused by the penetration of PVME. Both of them are most pronounced in 1 % solution. At higher concentration, the larger extent of deswelling leads to smaller mesh size of the network; this suppresses the permeability of PVME. On the other hand, the low concentration, whose gradient at the gel boundary is small, produces weaker driving force for the penetration. This dependence of the driving force agrees with the results in the previous work. In contrast, the characteristic time of the initial collapse is determined by the cooperative diffusion coefficient. This is the reason of the difference in the rate of the two processes.

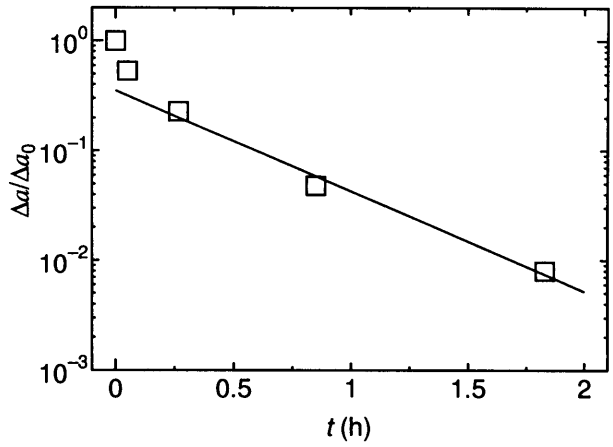

Figure 1.6: Semi-log plot of $\Delta a/\Delta a_0$ for the gel in 1 % solution. The dashed line is fitted to the data to obtain the characteristic time, τ, according to Eq. 1.1.

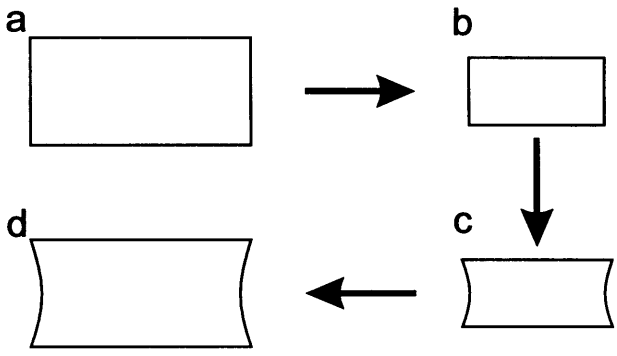

Figure 1.7: Schematic side view of disk-like gels. Swollen in pure water (a), collapsed in the solution (b), onset of re-swelling (c), and the re-swollen gel (d).

The molecular weight of solute polymers is important for the permeability as well. PVME with broad molecular weight distribution has sufficient amount of low-molecular-weight fraction. Although polyacrylamide and PVME are immiscible, they and water are miscible in the concentration range of the present work at room temperature [12]. There is good possibility for the penetration of PVME because of the existence of lower-molecular-weight fraction of PVME and the miscibility of the three components in spite of the immiscibility of the two polymers. The low molecular weight minimizes the loss of conformational entropy due to the penetration.

The shape of gels also indicates the entering of PVME (Fig. 1.7). After the initial collapse, the two bases of the disks first start to swell again. (Fig. 1.7c). They account for most of the gel boundary, through which PVME penetrates. This shape remained unchanged since its emergence. This is the evidence, considered with the thermodynamic analysis in the previous work, that the concentration of PVME is higher in the vicinity of two bases than the inner part.

The concentration dependence of the ultimate value of V/V_0 is an important problem. We have not finished the examination because of the slow process and hence the difficulty to determine them. It will be published in the near future.

The two peaks in the subtracted FTIR spectrum in Fig. 1.5 imply penetration of PVME though the other two peaks lack in it. This is possibly ascribed to the low concentration of PVME in the solution. It limits the inspection of the evidence for penetration of PVME.

References

[1] T. Tanaka, Phys. Rev. Lett., **40**, 820 (1978).

[2] T. Tanaka, D. J. Fillmore, S.-T. Sun, and I. Nishio, Phys. Rev. Lett., **45**, 1636 (1980).

[3] S. Hirotsu, Y. Hirokawa, and T. Tanaka, J. Chem. Phys., **87**, 1392 (1987).

[4] Y. Hirokawa, T. Tanaka, and S. Katayama, in "Microbial Adhesion and Aggregation", K. C. Marshall Ed., Springer-Verlag (1984).

[5] I. Ohmine and T. Tanaka, J. Chem. Phys., **77**, 5725 (1982).

[6] R. F. Boyer, J. Chem. Phys., **13**, 363 (1945).

[7] F. Brochard, J. Phys., **42**, 505 (1981).

[8] J. Bastide, S. Candau, and L. Leibler, Macromolecules, **14**, 719 (1981).

[9] J. Momii and T. Nose, Macromolecules, **22**, 1384 (1989).

[10] K. Adachi, T. Nakamoto, and T. Kotaka, Macromolecules, **22**, 3106 (1989).

[11] V. V. Vasilevskaya and A. R. Khokholov, Macromolecules, **25**, 384 (1992).

[12] T. Ikehara and T. Nishi, to be published.

[13] T. Tanaka and D. J. Fillmore, J. Chem. Phys., **70**, 1214 (1979).

[14] Y. Li and T. Tanaka, J. Chem. Phys., **92**, 1365 (1990).

[15] A. Peters and S. J. Candau, Macromolecules, **19**, 1952 (1986).

Chapter 2

Molecular mobility in gels

2.1 Introduction

Gels attract a lot of interest because of their drastic volume changes induced by the change of the environment they are placed. Ionized acrylamide gels, for example, undergo volume phase transition induced by the change in composition of the mixed solvent, temperature, pH, and salt concentration [1–5].

There have been several works on changes of molecular mobility and dynamics on volume phase transition [6–11]. Katayama *et al.* studied ionized acrylamide gels in acetone-water mixtures by electron paramagnetic resonance [6]. They observed discontinuous changes of molecular mobility at the transition point. Hu *et al.* studied microenvironment in acrylamide gels that undergo volume phase transition induced by pH and the composition of acetone-water mixtures [7–9]. They showed that molecules have sufficient mobility in the collapsed state near the transition point when the transition is induced by the change of pH [7]. There is also a deuterium NMR study of acrylamide gels [10]. A proton NMR study of *N*-isopropylacrylamide gels [11] revealed that main chains of the ionized samples are mobile in the collapsed state near the transition point, while those of the non-ionized ones are immobile. This was ascribed to the increased "stiffness" of the chains caused by the interaction with cations.

In these studies, molecular mobility was measured when the systems have reached the equilibrium state after the change of the environment. There have been fewer studies on dynamics during the volume phase transition process except a pulsed NMR study on the volume change process of acrylamide gels that do not undergo volume phase transition [12].

A rapid change of the environment not only causes contraction of gels, but also often produces heterogeneous structures inside the gels regardless whether they undergo volume phase transition This is because the shrinking rate, which is governed by the cooperative diffusion coefficient of the network [13, 14], is too small to follow the rapid change of the environment. In such a situation, the network forms sparse and dense regions to reduce total free energy of the system. It gains contact free energy by gathering the network chains in dense regions and the obtained energy compensates the entropic loss due to the heterogeneity. Gels with large dimensions often show the above behavior since it takes a long time for them to reach the equilibrium state [13, 14]. Li *et al.* treated this process as

spinodal decomposition using a turbidity technique [15].

Pulsed NMR is a powerful method to obtain the molecular mobility and the fractional amounts of heterogeneous phases in a sample. There are some examples applied to gels [16–18]. The main quantities obtained by pulsed NMR are the spin-spin relaxation time T_2, the spin-lattice relaxation time T_1, and that in the rotating frame $T_{1\rho}$. Since the time required for measurement is sufficiently shorter than that for the change in the system, especially for polymers, it enables us to analyze dynamics of the process. The signal of pulsed NMR for a heterogeneous system is superposition of different decay curves. One can obtain the mobility and the fractional amount of each phase by decomposing the signal. However, spin diffusion process causes energy transport between heterogeneous phases over a distance of several nanometers. This makes it ambiguous to determine the fractional amounts of heterogeneous phases in T_1 and $T_{1\rho}$ measurement [19]. Analyses of the transverse relaxation signals have been employed to decide the fractional amount for the above reason since the spin diffusion phenomenon has been considered unfavorable.

However, the spin diffusion process gives us information on the sizes of heterogeneous regions [20–22] using the Goldman-Shen pulse sequence [23]. This sequence first brings spin systems with different T_2 to different spin temperatures. Magnetization in the hard phase in a sample vanishes and that in the soft phase has a sufficient magnitude at this stage. The magnetization diffuses into the hard regions from the surrounding soft regions. After a certain diffusion time, the magnitude of magnetization in the hard phase is measured. One can obtain magnetization recovery curves in the hard phase with this procedure after several times of measurement with different diffusion time.

In this paper, we will discuss the properties of acrylamide gels in acetone-water mixture studied by pulsed NMR. After the measurement of concentration dependence of T_2, we investigated the change in molecular mobility during the volume phase transition process, both the shrinking and the swelling behavior. Domain sizes of heterogeneous phases caused by abrupt changes of the environment were also estimated with the Goldman-Shen pulse sequence. Relationship between microscopic environment, *i.e.*, molecular mobility and macroscopic volume is discussed.

2.2 Experimental

We used both ionized and non-ionized acrylamide gels in this study. The ionized samples were used for studies on the volume phase transition process and the neutral ones were used for studies on heterogeneous structures created by abrupt changes of the environment, *i.e.*, the composition of the solvent.

Ionized samples were composed with 19 g of the acrylamide monomer (main chain), 0.133 g of N,N'-methylene*bis*acrylamide (cross-linking agent), and 1.34 g of sodium acrylate (ionizing substance) in water. The total volume of the solution was 100 mℓ. Non ionized samples were composed with 20 g of the acrylamide monomer without sodium acrylate. After N,N,N',N'-tetramethylenediamine (initiator) and ammonium peroxodisulfate (accelerator) were added, gelation took place in tubes with different inner diameters and cylindrical samples were obtained. They were 3.7 mm for the volume change and phase transition experiments, and 1.55 cm for studies on heterogeneous structures. After the completion of gelation, the samples were immersed into a large amount of water to

wash away unreacted substances. Acetone-water mixtures were used as the solvent in the present experiment.

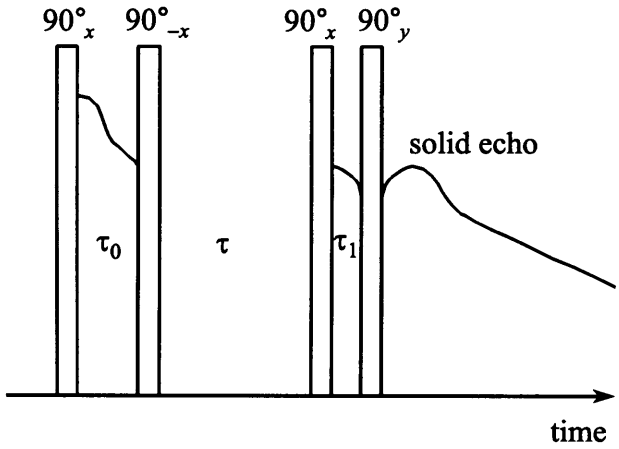

Figure 2.1: Schematic figure of the modified Goldman-Shen pulse sequence $(90°_x\tau_0 90°_{-x}\tau 90°_x\tau_1 90°_y)$. The spin diffusion takes place during the diffusion period τ.

The NMR instrument was Bruker PC-20 with the resonant frequency of 20 MHz for the proton. The signals were inputted into an A/D converter (FIXX FSA-1000SV) connected to a personal computer (NEC PC-9801VX). Spin-spin relaxation time T_2 was measured with the Carr-Purcell-Meiboom-Gill (CPMG) pulse sequence [24] in most of the experiments. The solid echo pulse sequence [25] was also applied to obtain information on the short-time behavior, if needed. The values of T_1 were measured by the inversion recovery pulse sequence for samples with heterogeneous structure. The signals were analyzed by the nonlinear least-square method. The modified Goldman-Shen pulse sequence [22] was employed for experiments on estimation of the sizes of heterogeneous structures. This sequence is a combination of the solid echo and the usual Goldman-Shen sequence to avoid the influence of the dead time. The schematic figure of this pulse sequence is shown in Fig. 2.1.

2.3 Results

Figure 2.2 shows the dependence of the swelling ratio V/V_0 (defined as the volume of the gel divided by that at gelation) of the neutral gel (a) and the ionized gel (b) on the volume percentage of acetone in the mixed solvent c. The volume phase transition occurred at $c = 49$ % for the ionized sample. The composition of the solvent was changed slowly to keep transparency and homogeneity of the networks. An example of a spin-spin relaxation decay of a non-ionized gel in the solvent with $c = 30\%$ is illustrated in Fig. 2.3. Figures 2.4 and 2.5 show the composition dependence of T_2 and the fractional amount f of each phase for the neutral and the ionized samples, respectively. The NMR signals were decomposed into two components for all c in both cases. Figure 2.6 shows the proton molar fraction of the solvent and the network calculated from the volume and mass for neutral (a) and

ionized (b) gels. Since the dependence of f in Fig. 2.4(b), Fig. 2.5(b), and Fig. 2.6 is almost the same, the components with the long T_2 (T_{2L}) and the short T_2 (T_{2S}) originate from the solvent and the network polymer, respectively.

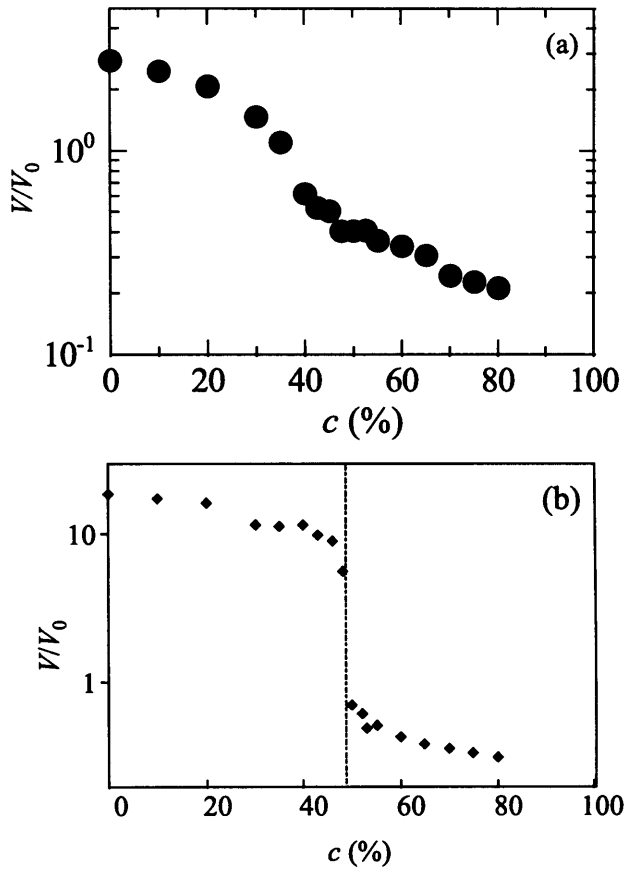

Figure 2.2: Dependence of the volume of the neutral gel (a) and the ionized gel (b) on acetone content of the solvent. The volume is reduced by that just after gelation.

The values of T_{2L} and T_{2S} decreased a little at the volume phase transition point for the ionized sample. This is because the shrinkage suppresses molecular mobility in the collapsed state. A more interesting result is that the mobility is further suppressed with increasing c, especially when $c > 70\%$, although the volume change in the collapsed state is much smaller than at the transition point (Figs. 2.2 and 2.5). The non-ionized gels exhibited the same behavior as shown in Figs. 2.2 and 2.4; although the neutral sample largely shrinks in the region where $20\% < c < 50\%$, the mobility is largely suppressed when $c > 50\%$.

Figure 2.7 shows the time evolution of V/V_0, T_2, and f in the shrinking process of an ionized gel. The sample that was first in the solvent with $c = 45\%$ was transferred into that with $c = 52.5$ % (Fig. 2.8). After the volume decreased a little in the early stage, it was almost constant for a short period, and then it decreased again. The period with the almost constant swelling ratio is called the plateau period [26]. This is attributed to the formation of a dense layer on the surface. After the relaxation of this structure during the

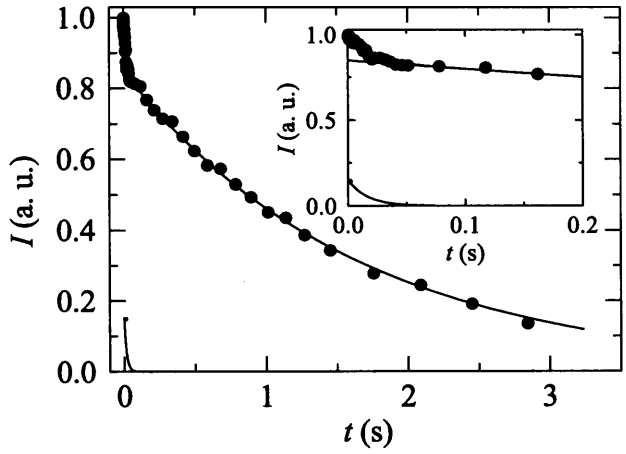

Figure 2.3: An example of a transverse relaxation decay curve (intensity I) decomposed into two components for a non-ionized gel in the solvent with $c = 30\%$. The dots are the data obtained by NMR and the lines are the fitted functions. The inset shows the short-time-range behavior.

plateau period, the volume further decreases. The value of T_2 of the solvent was almost constant in the early stage, then it decreased after the plateau period. The value of T_2 of the network polymer decreased constantly. The principal change in f took place after the plateau period (10^3 s $< t < 10^4$ s).

Figure 2.9 shows the time evolution of V/V_0, T_2, and f in the swelling process. The sample was transferred from the solvent with $c = 52.5\%$ into that with $c = 45\%$ (Fig. 2.8). Contrary to the shrinking process, T_2 of the solvent increased constantly although that of the polymer was almost constant in the early stage. The time range where T_2 of the network polymer increased coincided with that where the volume largely increased (10^2 s $< t < 10^3$ s). The principal change in f took place during the major increase of the volume as well.

The environment of non-ionized gels whose diameter at the gelation was 1.55 cm was rapidly changed to form heterogeneous structures. The experimental conditions, the results of spin-spin relaxation measurement, and the sample codes are summarized in Table 2.1. Since the inner and the outer parts of the heterogeneous samples were different in transparency and the texture, as schematically described in Fig. 2.10, they were measured separately. The signals of $S0_{in}$, $S0_{out}$, and $S35_{out}$ were decomposed into three components and the components with the shortest T_2 were Gaussian components, while the others were decomposed into two or three exponentially decaying components. Table 2.2 shows the proton molar fraction of the network polymer calculated from the mass of dried samples. Comparing the fractional amounts in Tables 2.1 and 2.2, we concluded that the fastest and the second fastest decaying components are assigned to the network polymer for $S0_{in}$ and $S35_{out}$, and that the Gaussian component is assigned to the network for $S0_{out}$. Table 2.3 shows the results of T_1 measurement performed on the three samples with a Gaussian component in the transverse relaxation. The spin-lattice relaxation had two components. The difference in the number of components for T_1 and

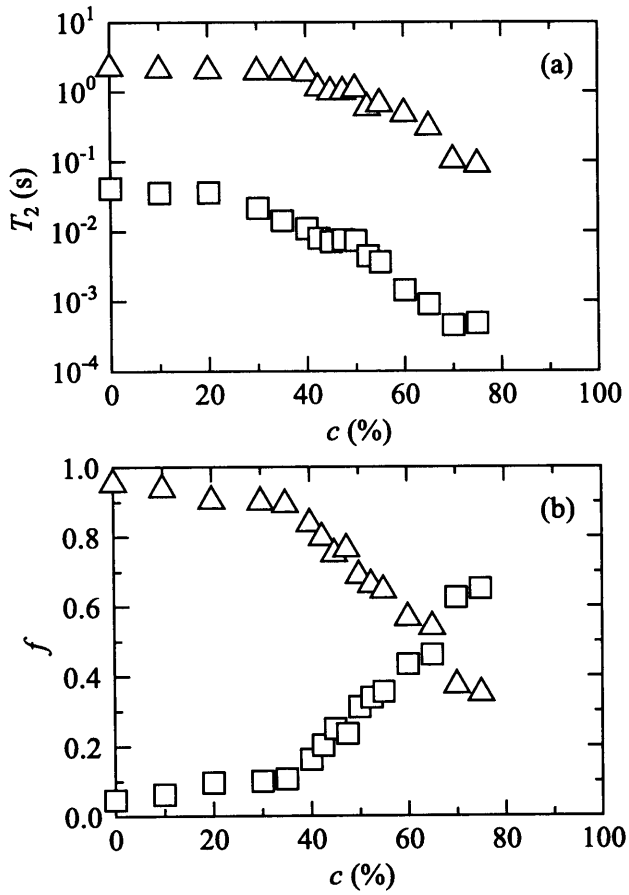

Figure 2.4: Dependence of T_2 (a) and fractional amount f (b) of each phase in the non-ionized gel on acetone content of the mixed solvent. The NMR signals were decomposed into two components.

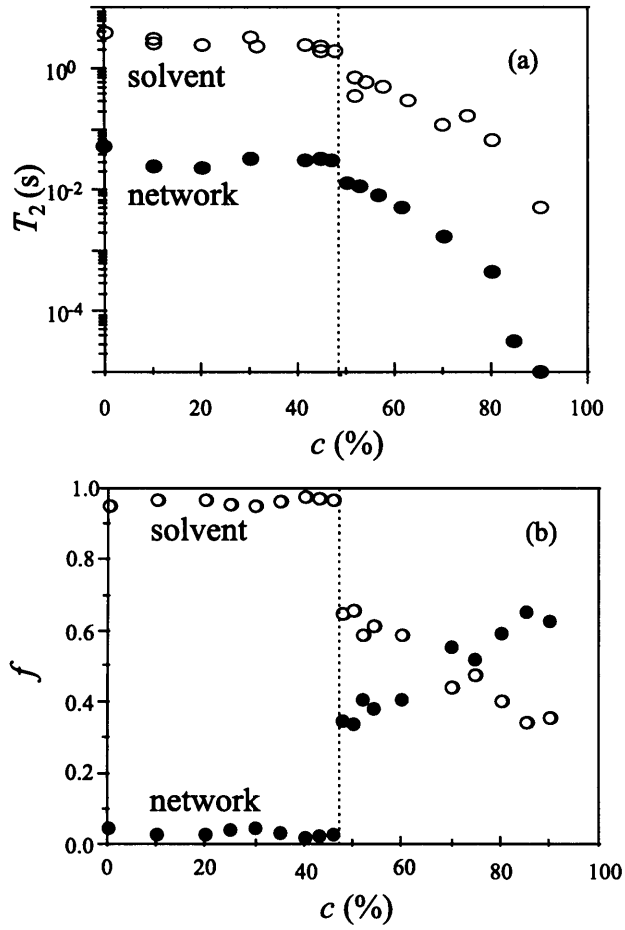

Figure 2.5: Dependence of T_2 (a) and fractional amount f (b) of each phase in the ionized gel on acetone content of the mixed solvent. The NMR signals were decomposed into two components.

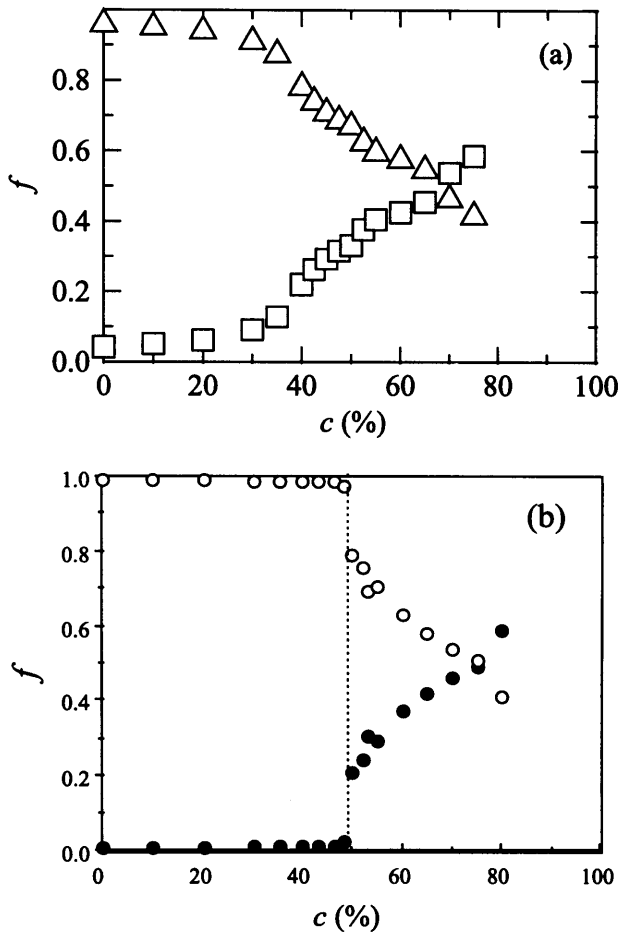

Figure 2.6: Proton molar fractions of the solvent and the network plotted against the acetone content of the mixed solvent for neutral (a) and ionized gels (b).

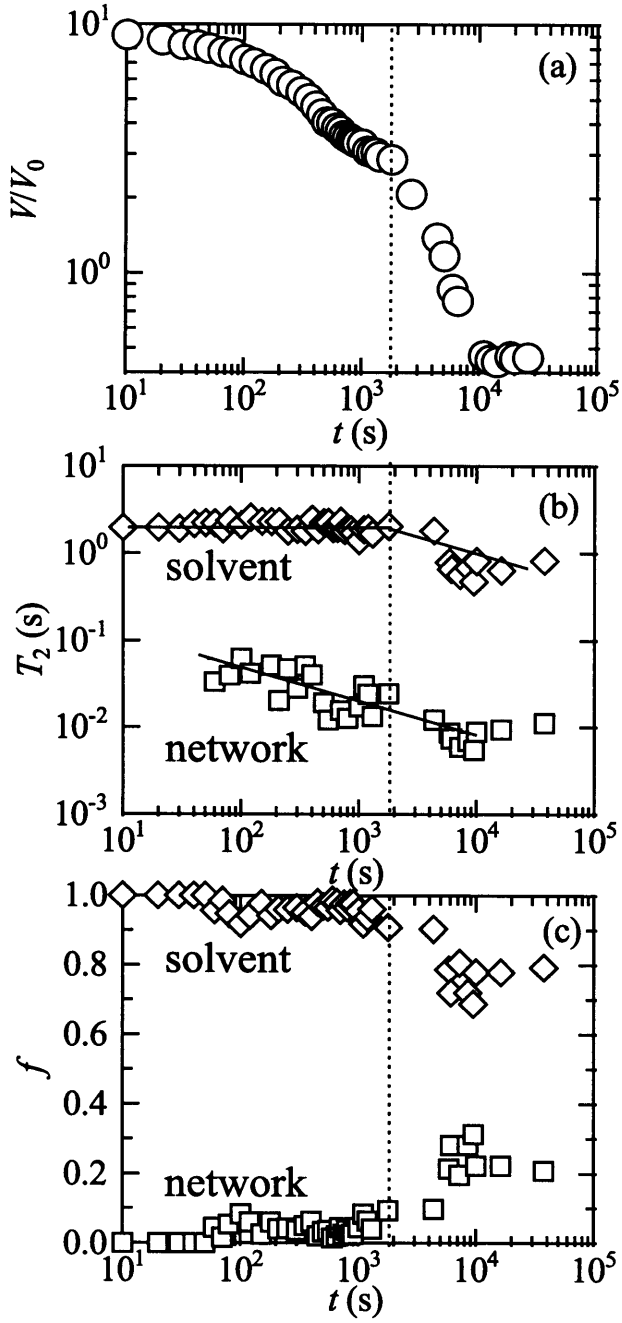

Figure 2.7: Time evolution of the swelling ratio (a), T_2 (b), and f (c) for the shrinking process of acrylamide gels. The sample was transferred from a solvent with $c = 45\%$ into that with 52.5%. The lines are the guides for the eye.

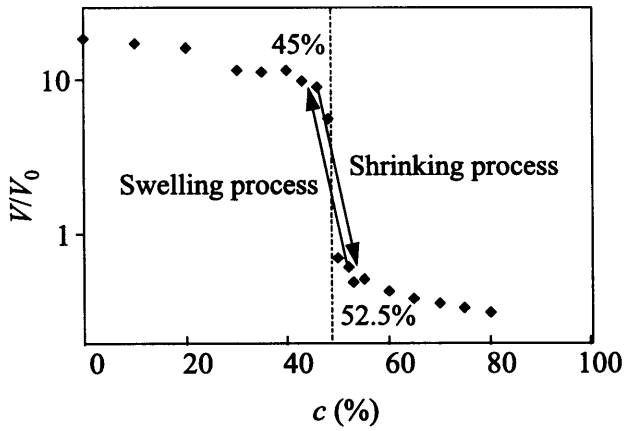

Figure 2.8: The conditions for the shrinking process and the swelling process of the ionized gel.

Table 2.1: Experimental conditions and the results of T_2 and the fractional amounts of heterogeneous samples. $c_{\text{init}} \rightarrow c_{\text{dest}}$ shows the initial and destination concentrations of the solvent. "G" in the component 1 shows that it is a Gaussian component.

Condition			Component 1	Component 2	Component 3	Transparency
0% → 60%	$M0_{in}$	T_2 (s)	1.5×10^{-3}	4.7×10^{-2}	3.2×10^{0}	turbid
		f (%)	25	55	20	
	$M0_{out}$	T_2 (s)	–	1.0×10^{-3}	2.0×10^{-1}	transparent
		f (%)	–	43	57	
35% → 60%	$M35_{in}$	T_2 (s)	2.7×10^{-3}	6.0×10^{-2}	3.5×10^{0}	turbid
		f (%)	23	48	29	
	$M35_{out}$	T_2 (s)	–	9.2×10^{-4}	1.6×10^{-1}	transparent
		f (%)	–	40	60	
0% → 100%	$S0_{in}$	T_2 (s)	7.1×10^{-6}	3.2×10^{-3}	6.8×10^{-1}	turbid
		f (%)	G40	26	34	
	$S0_{out}$	T_2 (s)	6.4×10^{-6}	1.8×10^{-3}	4.1×10^{-1}	turbid
		f (%)	G66	30	4	
35% → 100%	$S35_{in}$	T_2 (s)	–	1.7×10^{-2}	7.4×10^{0}	turbid
		f (%)	–	85	15	
	$S35_{out}$	T_2 (s)	6.8×10^{-6}	1.9×10^{-3}	3.1×10^{-1}	turbid
		f (%)	G50	20	30	

–: not observed

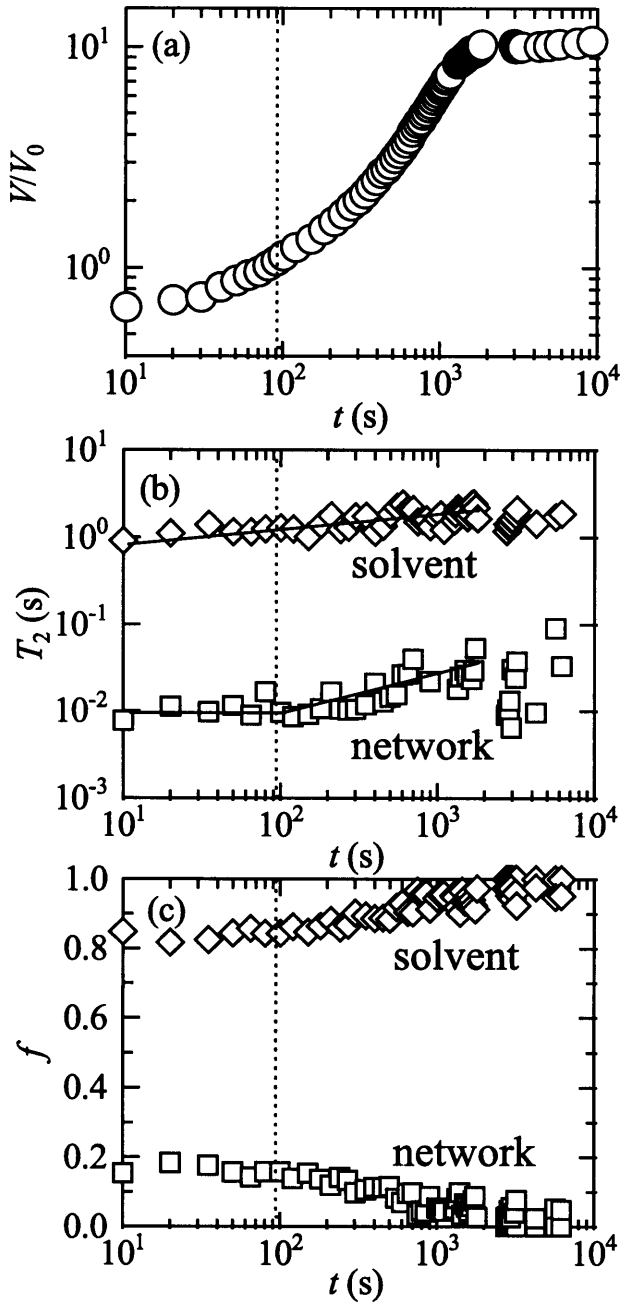

Figure 2.9: Time evolution of the swelling ratio (a), T_2 (b), and f (c) for the swelling process of acrylamide gels. The sample was transferred from a solvent with $c = 52.5\%$ into that with 45%. The lines are the guides for the eye.

Table 2.2: The proton molar fraction of the network (f_p) calculated from the mass of the dried samples.

Sample	$M0_{in}$	$M0_{out}$	$M35_{in}$	$M35_{out}$	$S0_{in}$	$S0_{out}$	$S35_{in}$	$S35_{out}$
f_p (%)	27	61	32	55	77	75	25	61

Table 2.3: Results of T_1 and the fractional amounts of heterogeneous samples that had a Gaussian component in the transverse relaxation.

		Component	
		1	2
$S0_{in}$	T_1 (ms)	104	1780
	f (%)	60	40
$S0_{out}$	T_1 (ms)	89.7	1250
	f (%)	91	9
$S35_{out}$	T_1 (ms)	93.9	1660
	f (%)	67	33

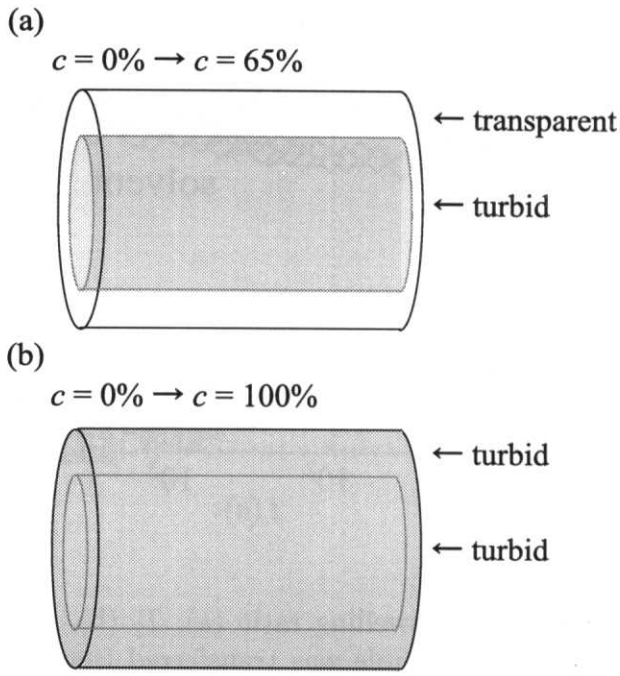

Figure 2.10: Schematic figure of the difference of the outer and inner parts of a cylindrical gel after an abrupt change of the environment for samples M0 (a) and S0 (b).

T_2 is ascribed to spin diffusion.

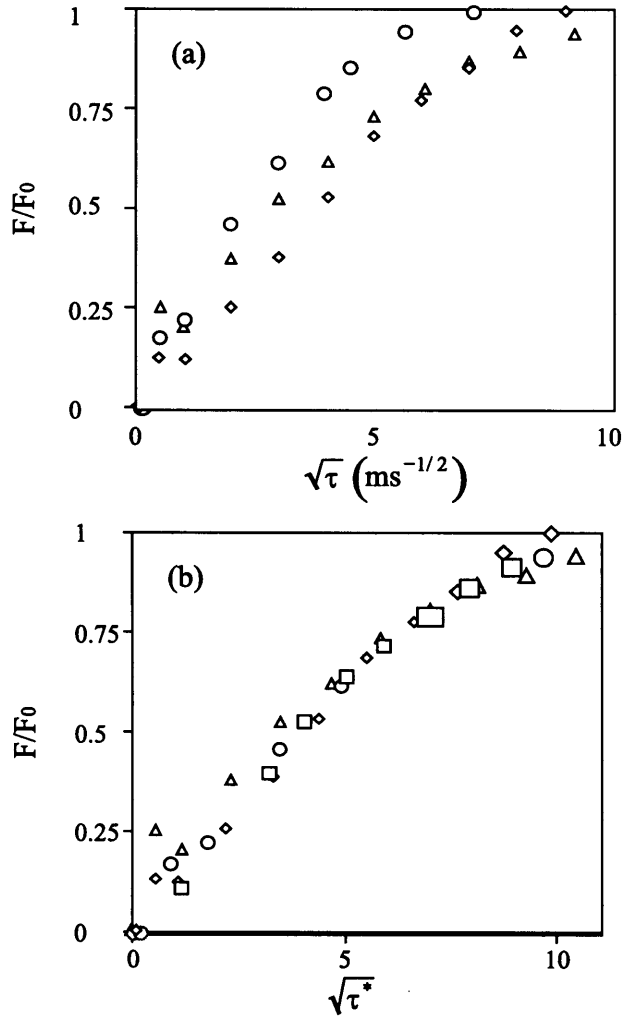

Figure 2.11: Recovery curves obtained by Goldman-Shen sequence from the samples (a) and those scaled to that of a block copolymer (b) for the samples $S0_{in}$ ($\diamond$), $S0_{out}$ ($\circ$), and S35 ($\triangle$). The symbol $\square$ in (b) is a recovery function of a block copolymer whose domain size is already known [22].

Figure 2.11(a) shows the recovery functions of magnetization in the hard phase obtained by the modified Goldman-Shen sequence. This experiment was performed on the three samples that had a fast decaying Gaussian component. The spin diffusion time τ of these curves was scaled by the characteristic time of diffusion $\tau^{*1/2} \equiv \tau^{1/2}/[L/(2dD)^{1/2}]$ as shown in Fig. 2.11(b), where L is the size of the hard phase, d is the spatial dimension, and D is the spin diffusion coefficient. The value of D is obtained as $D = 0.13{r_0}^2/T_2$ where r_0 is the lattice constant [27]. With the scaling factor $s = (\tau^*/\tau)^{1/2}$, the domain size of the hard phase in the gel was calculated with a reference recovery curve of a block copolymer whose domain size is already known (130 Å) [22]. The results are summarized in Table 2.4. It should be noted that, since these samples are opaque, it would be difficult to apply light scattering to estimate the domain sizes.

Table 2.4: Domain sizes of hard phases in heterogeneous gels.

Sample	Domain size (Å)
$S0_{in}$	120
$S0_{out}$	50
$S35_{out}$	60

2.4 Discussion

2.4.1 Concentration dependence of T_2

The transverse relaxation signals were decomposed into two components (the solvent and the network polymer) for both ionized and non-ionized samples for all c (Figs. 2.4 and 2.5). There must exist two states for the solvent molecules: those bound by the network and the free molecules. However, these two states were not detected by the pulsed NMR although the molecular mobility must be different from each other. This is ascribed to the fast exchange of solvent molecules between the two states. The observed spin-spin relaxation time ${T_2}^{(\mathrm{obs})}$ is described as ${T_2}^{(\mathrm{obs})^{-1}} = f^{(1)}/{T_2}^{(1)} + f^{(2)}/{T_2}^{(2)}$, where $f^{(i)}$ and ${T_2}^{(i)}$ are the fractional amount and T_2 in the state i, respectively [28]. When gels are swollen and contain a lot of solvent inside, ${T_2}^{(\mathrm{obs})} \simeq {T_2}^{(\text{free solvent})}$ since most of the solvent molecules are unbound.

As shown in Figs. 2.2, 2.4, and 2.5, molecular mobility is more suppressed in the collapsed state ($c > 50\%$ for the non-ionized gel and $c > 70\%$ for the ionized gel) than in the concentration region where large collapse takes place ($30\% < c < 50\%$ for the non-ionized gel and $c = 49\%$ for the ionized gel). There are two factors considered that suppress molecular mobility: volume of the system and the interaction parameter between the chains and the solvent. The results indicate that the interaction parameter has more influence on molecular mobility than the volume of the system. As the mobility of the network polymer is suppressed, that of the solvent trapped in the mesh is also suppressed. Another possible reason is that, in the present experiment, the solvent is a mixture of acetone and water. A sufficient amount of water persists in the solvent around the volume phase transition point. These water molecules interact with the network chains. There is good possibility that they increase the mobility. Molecular mobility detected by NMR reflects the local environment. One cannot discuss the mobility only with the volume itself. In the present case, further discussions should be based on the ternary system of the polymer, water, and acetone.

There are a few works that showed the network polymers have sufficient mobility in the collapsed state near the transition point [7, 11]. Tokuhiro *et al.* compared ionized and non-ionized *N*-isopropylacrylamide gels and concluded that the ionization increases molecular mobility in the contracted gels. In the present study, however, the network chains of both ionized and non-ionized samples are mobile in the collapsed state. This indicates that the influence of ionization on the enhancement of mobility is small in our case.

2.4.2 Shrinking and swelling dynamics

Dynamics of the shrinking and swelling process is different from each other as shown in Figs. 2.7 and 2.9. In the shrinking process, the response of the network chains is faster than that of the solvent. In the swelling process, on the other hand, the response of the solvent is faster than that of the polymer. This reflects the behavior that the swelling and shrinking start on the boundary of the samples as discussed below.

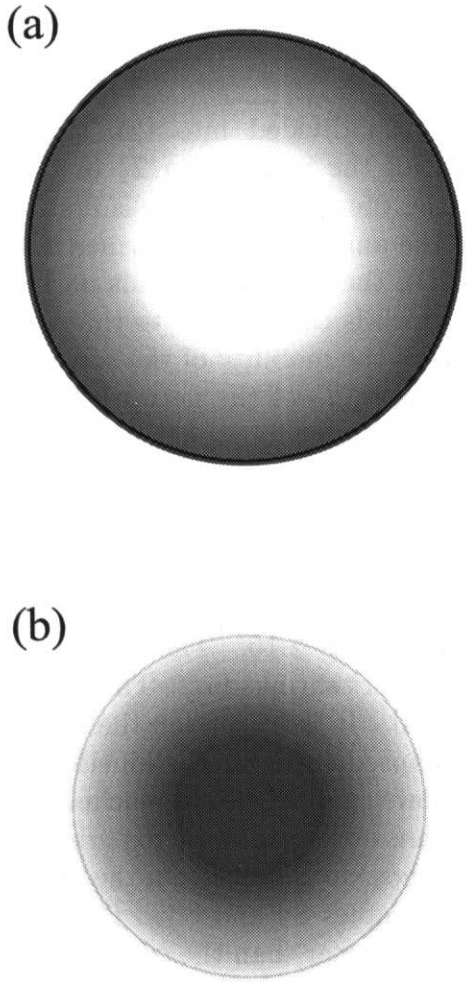

Figure 2.12: Schematic cross sections of the gels in the shrinking process (a) and the swelling process (b). The gray scale shows the density of the network; the shaded part is collapsed and the white part is swollen.

The shrinking process is divided into two stages: before the end of the plateau period (stage I) and after the end of this period (stage II). In stage I, where only the outer part of the gel shrinks (Fig. 2.12(a)), T_2 of the solvent is almost constant and that of the polymer decreases. There are several factors to explain this behavior. The reason for the fast response of the network is that, when a gel is transferred from a good solvent to a poor one, the polymer chains contact to each other to reduce contact free energy and, hence, the mobility of the polymer is lowered. The density of the network chains is larger

in the outer part than in the inner part. The difference in mobility of the chains between the inner and outer parts is not large enough for pulsed NMR to decompose. The decrease in T_2 for the chains reflects the superposition of the increasing amount of immobile chains (outer part) and the decreasing amount of mobile ones (inner part). The reason for the almost constant T_2 of the solvent in stage I is the presence of a lot of free (unbound) solvent molecules in the swollen inner part. Pulsed NMR again cannot decompose the signals of the solvent in the collapsed and still swollen networks. In stage II, where the volume further decreased, the decrease in T_2 of the solvent reflects the increasing amount of the bound molecules and decreasing amount of the free molecules in the shrinking process.

The swelling process is also divided into two stages: before (stage I′) and after (stage II′) the beginning of the increase in T_2 of the network. In stage I′, where the total volume changes little, the outer part swells first, while the inner part is still collapsed (Fig. 2.12(b)). Since the amount of the polymer in the outer swollen part is small, the total T_{2S} changes little. On the other hand, this part contains a sufficient amount of the solvent, the amount of which is comparable to that in the inner part. The solvent in the swollen outer part increases the mobility of the solvent in stage I′. In stage II′, where the total volume largely increases, T_2 of the network begins to increase. As the volume increases, the amount of mobile chains in swollen networks increases.

2.4.3 Heterogeneous structure

Transparency and the texture of the inner and the outer parts of the heterogeneous samples were different as shown in Fig. 2.10. The difference is ascribed to the shrinking behavior of gels that the outer part shrinks first. This is a consequence of the cooperative diffusive motion of gels [13, 14]. It is easier for the outer part than the inner part to approach the equilibrium collapsed state for the kinetic reason. The transparency of the samples $M0_{out}$ and $M35_{out}$ shows that they have reached the equilibrium state. This is reflected by the results of the transverse relaxation experiment on these samples (Table 2.1). They are almost the same as those in Fig. 2.4. On the other hand, both the outer and the inner parts were opaque for samples S0 and S35. However, the textures were different; the inner parts were softer and coarser than the outer parts. The reason for the difference is described as follows: the abrupt change of the environment makes the contracted outer part hard enough to prevent further collapse. The inner part still contains a sufficient amount of the poor solvent to which the hard outer part is impermeable. The excess amount of the poor solvent in the inner part forces more network chains to contact to each other to reduce the contact free energy between the polymer and the solvent. This is reflected by the difference in the domain sizes of $S0_{in}$ and $S0_{out}$ (Table 2.4).

The fast collapse of the outer part also explains that $S35_{in}$ has only two components in the transverse relaxation. Since the volume of the non-ionized sample in the solvent with $c = 35\%$ is smaller than in the pure water by 40% (Fig. 2.2), its mesh size is also smaller. When it is soaked into pure acetone, the immediate collapse of the outer part hinders the exchange of the solvent in the inner part. The two components of $S35_{in}$ are the consequence of the less poor solvent in the inner part.

The transverse relaxation curves of $S0_{in}$, $S0_{out}$, and $S35_{out}$ were decomposed into three

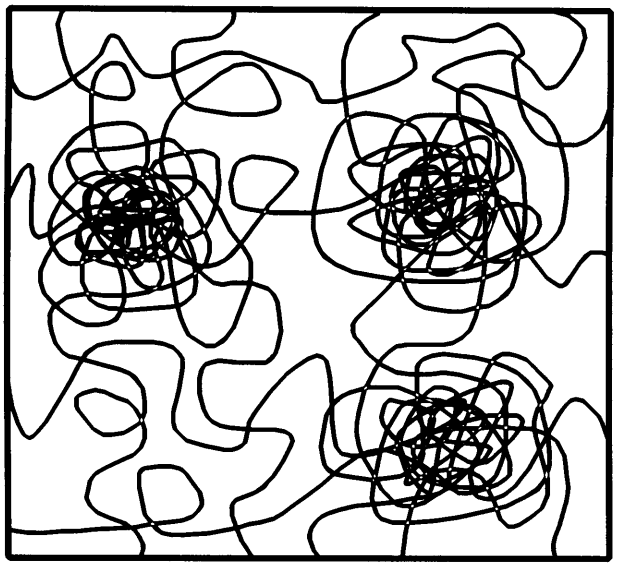

Figure 2.13: A schematic figure of the network structure of a heterogeneous gel.

components (Table 2.1). The component whose T_2 is of the order of 10^{-5} s is assigned to a solid-like state in the heterogeneous structure. On the other hand, the solvent molecules, which have long T_2, are divided into two types: one is those in the dense region of the network and the other is those in the sparse region (Fig. 2.13). There is little possibility that these regions frequently exchange the solvent molecules and that it has sufficient influence on the transverse relaxation behavior. The most mobile component, therefore, is assigned to the solvent in the sparse regions and a part of the intermediate component is assigned to that in the dense regions. In both regions, there are unbound and bound solvent. A large fraction of the solvent in the sparse regions is unbound and only a small fraction is bound by the network. The situation is the opposite in the dense regions.

Gels with heterogeneous structure are white and turbid. The reason for the turbidity is that light is scattered by the heterogeneity in the refractive index in the sample. This indicates that the dimension of the heterogeneous structure is comparable to the wave length of visible light. The results of the size of the hard phase obtained by the Goldman-Shen experiment is smaller than is estimated from this consideration. This is because the hard phase detected by pulsed NMR is on a smaller scale. The heterogeneous structure detected by light scattering is heterogeneity of the gel itself (network chains and the solvent). However, the hard phase detected by the solid echo pulse sequence is a smaller solid-like structure whose T_2 is of the order of 10^{-5}. Solid-like regions that are aggregations of only the chains appear in the dense phase in Fig. 2.13.

We now discuss the influence of the interface between the hard solid-like regions and the surrounding soft regions. Figure 2.14 shows two types of interfaces: one is that with a gradual change of the structure in a real system (Fig. 2.14(a)) and the other is an ideal stepwise structure (Fig. 2.14(b)). After the magnetization in the hard phase is eliminated by the Goldman-Shen sequence, the interface still has appreciable magnetization since T_2 in this phase is longer than that in the hard phase. Only the boundaries of the hard

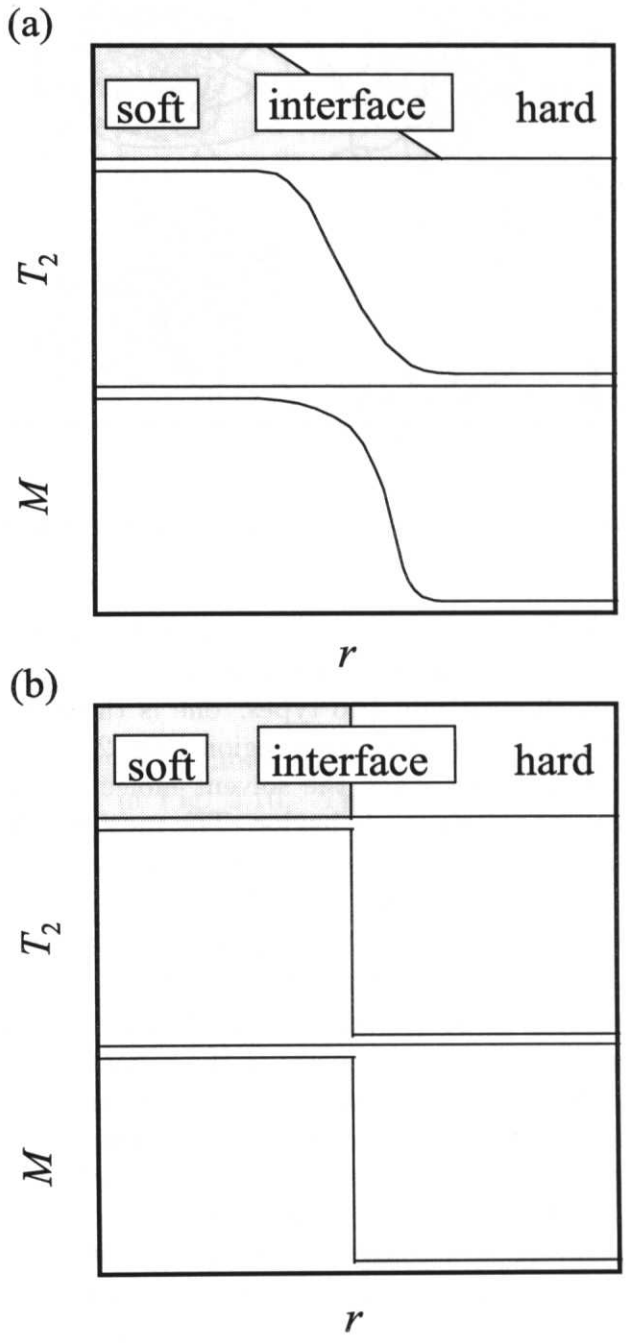

Figure 2.14: Spatial profiles of T_2 and the magnetization after the second pulse ($90°_{-x}$) in the Goldman-Shen sequence for a real system (a) and an ideal system (b).

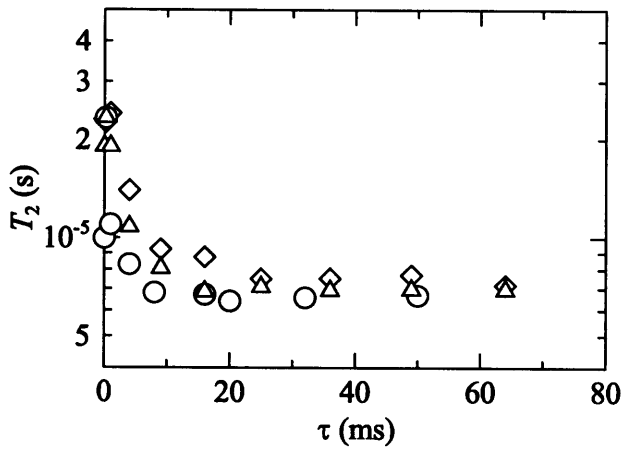

Figure 2.15: Dependence of T_2 of the hard phases on the spin diffusion time τ. Symbols are identical with those in Fig. 2.11.

regions have magnetization for a short diffusion time τ. Since they are less perfect than the hard phase, the value of T_2 for the hard phase is longer for small τ than that for large τ as shown in Fig. 2.15. Moreover, the interfacial phase contains a small amount of solvent molecules. The origin of spin diffusion is spin flip-flop motion through the dipole-dipole interaction of nuclei. The polymeric systems the Goldman-Shen sequence has been applied to so far contained only polymer molecules and no low molecular-weight substances like solvent [20–22]. In such situations, one has to consider intra- and intermolecular spin diffusion in polymers. In the present study, however, the self-diffusion of the solvent molecules must be taken into account. This effect enhances the magnetization recovery in the hard phase. The obtained dimensions may be smaller than the actual dimensions.

References

[1] T. Tanaka, Phys. Rev. Lett., **40**, 820 (1978).

[2] T. Tanaka, D. J. Fillmore, S.-T. Sun, and I. Nishio, Phys. Rev. Lett., **45**, 1636 (1980).

[3] S. Hirotsu, Y. Hirokawa, and T. Tanaka, J. Chem. Phys., **87**, 1392 (1987).

[4] Y. Hirokawa, T. Tanaka, and S. Katayama, in "Microbial Adhesion and Aggregation," K. C. Marshall Ed., Springer-Verlag (1984).

[5] I. Ohmie and T. Tanaka, J. Chem. Phys., **77**, 5725 (1982).

[6] S. Katayama, S. Kazama, and H. Yoshioka, J. Phys. Chem., **96**, 2023 (1992).

[7] Y. Hu, K. Horie, H. Ushiki, F. Tsunomori, and T. Yamashita, Macromolecules, **25**, 7324 (1992).

[8] Y. Hu, K. Horie, and H. Ushiki, Macromolecules, **25**, 6040 (1992).

[9] Y. Hu, K. Horie, H. Ushiki, T. Yamashita, and F. Tsunomori, Macromolecules, **26**, 1761 (1993).

[10] M. Corti, L. Pavesi, A. Rigamonti, and F. Tabak, Phys. Rev. A, **43**, 6887 (1991).

[11] T. Tokuhiro, T. Amiya, A. Mamada, and T. Tanaka, Macromolecules, **24**, 2936 (1991).

[12] T. Hayashi, Y. Urai, J. Inoue, T. Ikehara, and T. Nishi, Rept. Prog. Polym. Phys. Jpn., **35**, 499 (1992).

[13] T. Tanaka and D. J. Fillmore, J. Chem. Phys., **70**, 1214 (1979).

[14] Y. Li and T. Tanaka, J. Chem. Phys., **92**, 1365 (1990).

[15] Y. Li, G. Wang, and Z. Hu, Macromolecules, **28**, 4194 (1995).

[16] H. Tanaka, K. Fukumori, and T. Nishi, J. Chem. Phys., **89**, 3363 (1988).

[17] T. Shiga, K. Fukumori, Y. Hirose, A. Okada, and T. Kurauchi, J. Polym. Sci. B, Polym. Phys., **32**, 85 (1994).

[18] F. Tabak, M. Corti, L. Pavesi, and A. Rigamonti, J. Phys. C, **20**, 5691 (1987).

[19] D. C. Douglass and V. J. McBrierty, J. Chem. Phys., **54**, 4085 (1971).

[20] R. A. Assink, Macromolecules, **11**, 1233 (1978).

[21] T. T. P. Cheung, J. Chem. Phys., **76**, 1248 (1982).

[22] H. Tanaka and T. Nishi, Phys. Rev. B, **33**, 32 (1986).

[23] M. Goldman and L. Shen, Phys. Rev., **144**, 321 (1966).

[24] S. Meiboom and D. Gill, Rev. Sci. Instrum., **29**, 688 (1958).

[25] J. G. Powles and J. H. Strange, Proc. Phys. Soc. London, **82**, 6 (1963).

[26] E. S. Matsuo and T. Tanaka, J. Chem. Phys., **89**, 1695 (1988).

[27] T. T. P. Cheung, B. C. Gerstein, L. M. Ryan, R. E. Taylor, and C. R. Dybowski, J. Chem. Phys., **73**, 6059 (1980).

[28] J. R. Zimmermann and W. E. Brittin, J. Phys. Chem., **61**, 1327 (1957).

Part II

Dynamics of the Crystallization of Polymers

Chapter 3

Crystallization process in polymer blends

3.1 Introduction

Pulsed NMR, among various methods to investigate the crystallization process of polymers [1–3] and polymer blends [4,5], is not widely employed so far in spite of its advantages. It is able to obtain information on heterogeneous phases such as molecular mobility and the fractional amounts in the system. When the crystallization process is slow enough compared with the rate of one measurement routine, it is possible to investigate in-situ crystallization process of crystalline polymers, which have intrinsic heterogeneity inside, from a melt in the temperature-controlled NMR probe. The spin-spin relaxation time T_2 is mostly employed to obtain the information on a system where small domains of low molecular mobility are dispersed since spin diffusion often loses the information in the measurements of the spin-lattice relaxation time T_1 and the spin-lattice relaxation time in the rotating frame $T_{1\rho}$.

Melt crystallized polymers exhibit the morphology of lamella-stack crystals, in which immobile crystals, mobile amorphous, and intermediate interfacial zones coexist. Pulsed NMR is able to analyze the behavior of the three states individually by decomposing relaxation curves. One of the features of pulsed NMR is the ability to obtain the information relatively easily on the interface [6–12]. A detailed discussion of the crystallization process of poly(ϵ-caprolactone) (PCL) analyzed by pulsed NMR is found elsewhere [12]. The possibility of detection of the pre-ordering state in the early stage of the crystallization process was discussed for PCL blended with oligostyrene (OS) [13].

Crystallization of polymers can be divided into two processes, namely primary and secondary crystallization. Spherulites grow outward until they collide with neighbors in the primary process, while lamellar thickening, crystallization of interlamellar amorphous chains, and the changes of lamellar structure occur in the secondary process. The slow rate and the required long period for measurement of the secondary process make the detailed studies still insufficient in spite of its importance.

An amorphous polymer acts as impurities in crystalline/amorphous polymer blends. The mixed impurities cause melting temperature depression, changes in morphology, and the decrease of the spherulite growth rate. The amorphous polymer is rejected from the

crystals into interlamellar, interfibrillar, and interspherulitic regions [14].

There are works on the crystallization process of PCL/OS blends as a crystalline/amorphous blend system by optical microscopy [15] and time-resolved x-ray diffraction [16, 17]. They mainly focused on the changes of the structures during crystallization. On the other hand, pulsed NMR analyzes the process from the view point of molecular mobility. It also enables us to examine the secondary crystallization process when the measurement is continued for a sufficiently long time after the completion of the primary process. Local phase separation during crystallization was also discussed in the works by optical microscopy [15] and x-ray diffraction [18].

The aim of the present paper is to analyze the crystallization process of crystalline/amorphous polymer blends, PCL/OS, by measuring T_2 by pulsed NMR. We examined the temporal changes of the crystalline, amorphous, and intermediate components in the crystallization process and the dependence of the behavior on the crystallization temperature and the amorphous polymer content. We also report the behavior in the primary and secondary crystallization process, the relation with the morphology of spherulites, and the possibility of local phase separation.

3.2 Experimental

The characteristics of the polymers are displayed in Table 3.1. The equilibrium melting temperatures of the blends determined by the Hoffman-Weeks plot [19] are shown in Table 3.2. The phase diagram of the blends is shown in Fig. 3.1 along with the melting point depression curve. Since the depression was small, we used temperature itself for displaying the results of temperature dependence instead of the degree of supercooling, which is usually used for analyzing data.

Table 3.1: The characteristics of the samples in this work. Here, M_n is the number average molecular weight, M_w is the weight average molecular weight, T_m^0 is the equilibrium melting temperature, and T_g is the glass transition temperature.

Sample	Source	M_n	M_w	T_m^0 (K)	T_g (K)
PCL	Scientific Polymer Products	9300	14600	333	213
OS	Tohso	836	946		288

Table 3.2: Equilibrium melting temperature obtained by the Hoffman-Weeks plot.

OS content (%)	T_m^0 (K)
0	332.7
10	332.6
20	332.2
30	331.4

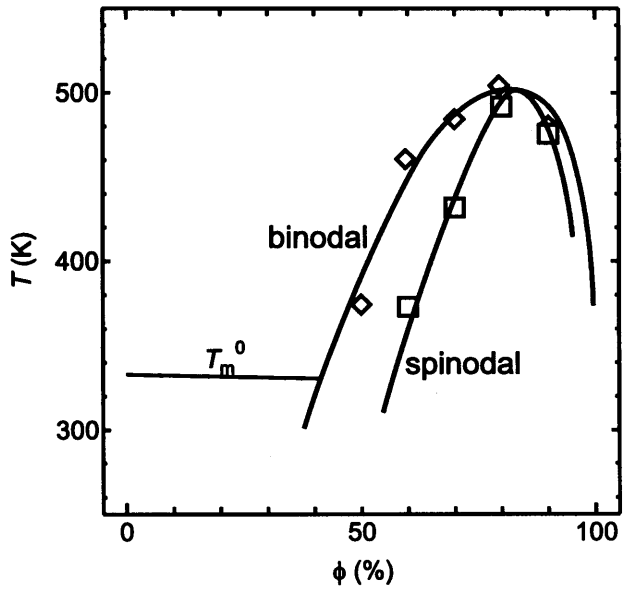

Figure 3.1: The phase diagram of the PCL/OS blends showing binodal and spinodal points. The lines are the guide for the eye. It also shows the melting point depression line.

Table 3.3: The experimental conditions of the crystallization temperature T_c, the blend composition ϕ_{OS} and the sample codes. The experiments were carried out under the conditions marked by circles, and not performed under the conditions marked by crosses.

		T_c (K)	308	312	315	318
Sample code	ϕ_{OS} (%)					
OS0	0		o	o	o	o
OS1	1		o	o	o	o
OS5	5		o	o	o	×
OS10	10		o	o	o	×
OS20	20		o	o	o	×
OS30	30		o	o	×	×

A blend in an NMR sample tube was melted above the melting point of PCL for more than one hour, then transferred into the NMR probe head whose temperature was kept at an experimental crystallization temperature. This moment is the time origin of the crystallization time t. Then, T_2 signals were acquired at desired t with solid echo and CPMG pulse sequences. The signals were analyzed by the nonlinear least square fitting method and we obtained the values of T_2 and the fractional amounts of the components. The crystallization temperature T_c, the OS content ϕ_{OS}, and the sample codes are displayed in Table 3.3. The crystallization process was too slow to obtain satisfactory data for high OS content samples at high T_c. Optical microscopy showed that no phase separation took place under the present conditions. The other details of the experiments are described elsewhere [13].

We measured T_2 of the samples crystallized for three days ($\equiv t_t$) and employed these data as the terminal value of the secondary crystallization process though crystallinity was still changing gradually at this point.

3.3 Results

Figure 3.2 is an example of a transverse relaxation signal decomposed into three components (one Gaussian and two exponential curves). The components of short, intermediate, and long T_2 were assigned to the crystalline, interfacial, and amorphous components, respectively as described in the works on crystalline polymers [6–12]. OS in the blend samples is rejected from the crystals during the crystallization process. It is mixed with amorphous PCL or trapped in the interfaces as discussed later. The components with the longest and intermediate T_2 of the blend samples therefore contain the contributions of rejected OS. In Fig. 3.3, T_2 of pure OS is plotted against temperature. Molecular mobility of OS is lower than that of the intermediate and amorphous components and is close to that of the crystalline phase under the conditions of the present paper. However, when OS is mixed with PCL in amorphous regions and interfaces on the molecular level, the signals of PCL and OS were not decomposed and were fitted with one component in the signals of pulsed NMR.

Examples of the temporal change of T_2 and the fraction f are shown in Fig. 3.4 for OS0 crystallized at 315 K and OS30 crystallized at 312 K. The transverse relaxation curve of the amorphous melt exhibited only one exponential component before the onset of crystallization. The signals have contributions both from PCL and OS melt for $\phi_{OS} > 0$. After the induction period, the crystalline component of OS0 emerged at $t_i \simeq 5 \times 10^2$ s. The slope of the crystalline component changed at $t_p \simeq 2 \times 10^3$ s; this is the boundary of the primary and secondary crystallization processes. The boundaries of t are schematically shown in Fig. 3.5. The fraction of the crystal f_c and the amorphous component f_a rapidly increased and decreased in the primary process, respectively. In the secondary process, f_c and the fraction of the intermediate component f_i increased gradually, while f_a decreased. The values of T_2 of all the components decreased slowly. The concave shape of f_i of OS30 in the early stage of crystallization is discussed elsewhere [13].

Figure 3.6 shows the dependence of T_2 on T_c and ϕ_{OS}. The values of T_2 of the intermediate and amorphous components increased with T_c and decreased with increasing ϕ_{OS}. The dependence of f for OS5 on T_c at t_p is displayed in Fig. 3.7. This figure shows that

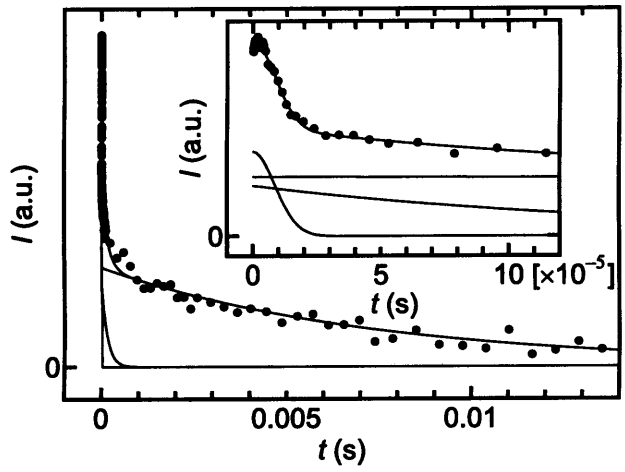

Figure 3.2: An example of a transverse relaxation signal decomposed into three components. $\phi_{OS} = 10$ %, $T_c = 312$ K, and $t = 3.2 \times 10^3$ s.

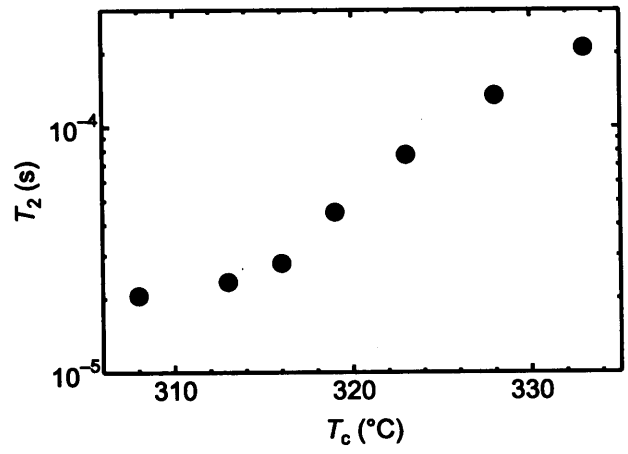

Figure 3.3: Temperature dependence of T_2 of oligostyrene.

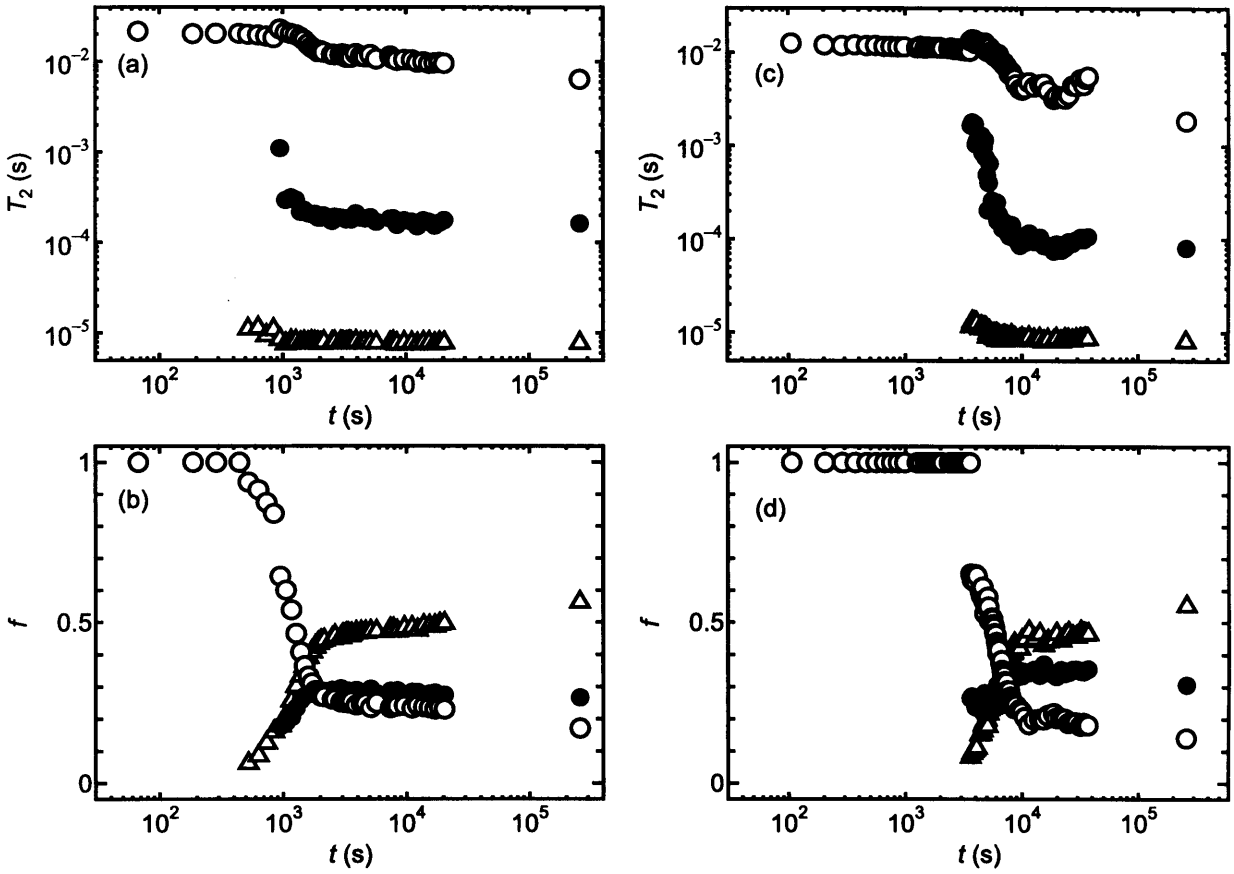

Figure 3.4: Examples of the temporal changes of T_2 and f. (a) T_2 and (b) f of pure PCL crystallized at 315 K. (c) T_2 and (d) f of the $\phi_{OS} = 30\%$ blend crystallized at 312 K. ○ amorphous, △ crystalline, and • intermediate components.

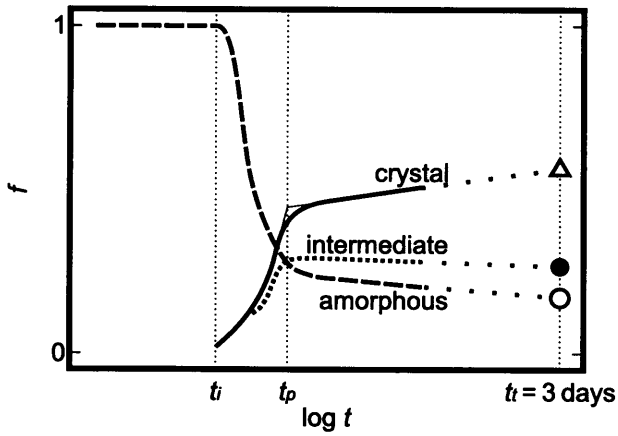

Figure 3.5: A schematic figure of the temporal change of the fractional amounts of the components measured by pulsed NMR and notations of the time of the boundary in the process: t_i is the time when the crystalline component emerges, t_p is the time of the boundary of the primary and secondary crystallization process, and t_t is the terminal crystallization time of this paper (three days).

f_c and f_i decrease with increasing T_c while f_a increases.

Figures 3.8–3.10 display in detail the dependence of f on T_c and ϕ_{OS}. The values both at t_p and t_t are shown in Figs. 3.8 and 3.9. The data only at t_p are shown for the intermediate component since the changes of f_i were not large enough between at t_p and at t_t.

Figure 3.11 shows the polarized optical micrographs of the spherulites of the samples. As ϕ_{OS} increased, spherulites gradually showed fibrillar structures for $\phi_{OS} \gtrsim 5\%$. This indicates that the impurities started to be rejected into the interfibrillar regions at 5%.

3.4 Discussions

3.4.1 Changes of T_2

In the primary process, T_2 of the three components decreased as shown in Fig. 3.4. These results indicate that the progress of crystallization suppresses molecular mobility in all the three components. The suppression of mobility of the crystalline and intermediate components with time is attributed to the perfection of the crystalline structure, i. e., crystals with fewer defects inside have lower mobility and they also suppress the mobility in the connected interfaces. The situation of the amorphous phase is different. It consists of the relatively mobile amorphous melt outside the spherulites and the relatively immobile interlamellar amorphous chains constrained by lamellae. The difference in T_2 of the amorphous melt and the interlamellar amorphous chains is too small for pulsed NMR to decompose their signals. The decrease of T_2 of the amorphous phase in the primary process is a consequence of the decrease of the amount of the amorphous melt and the increase of that of the interlamellar amorphous chains. The gradual decrease of T_2 of the interfacial and amorphous components in the secondary process suggests some structural

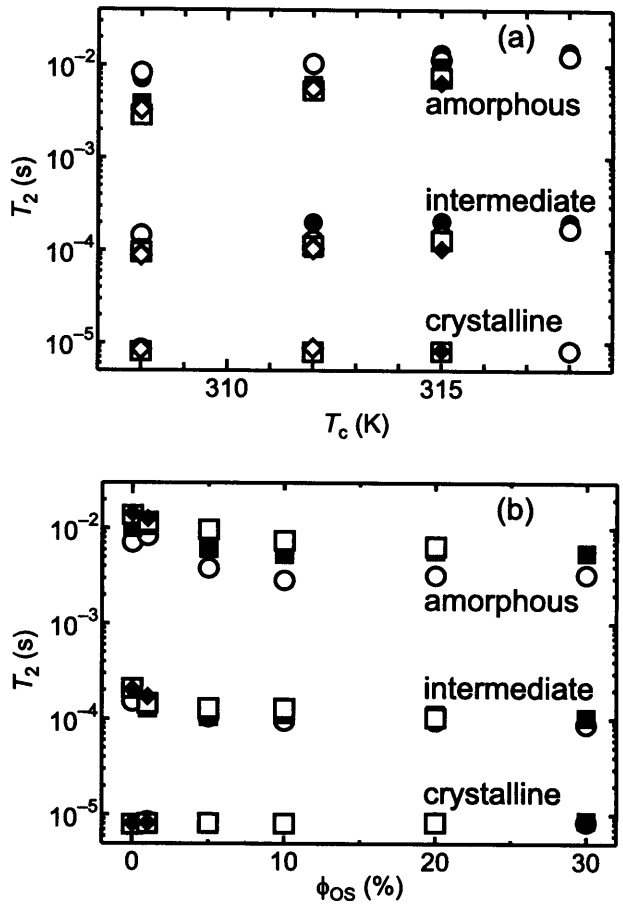

Figure 3.6: Dependence of T_2 on (a) T_c and (b) ϕ_{OS} at the end of the primary crystallization process. (a) • $\phi_{OS} = 0\%$, ○ 1%, ■ 5%, □ 10%, ♦ 20%, and ◇ 30%. (b) ○ $T_c = 308$ K, ■ 312 K, □ 315 K, and ♦ 318 K.

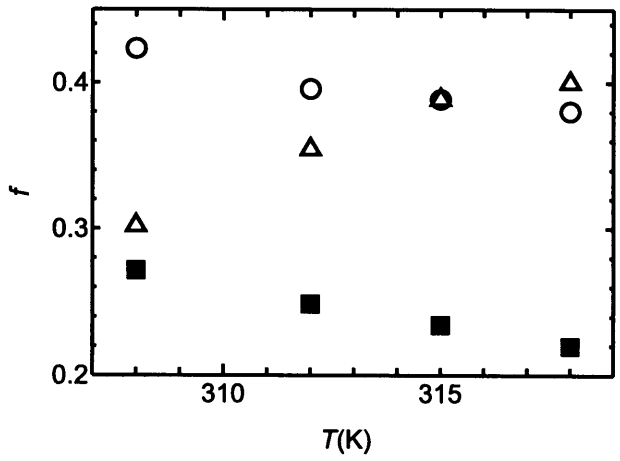

Figure 3.7: Crystallization temperature dependence of the fractional amount of each component, ○ crystal, ■ intermediate, and △ amorphous, of a ϕ_{OS} 5% sample at t_p.

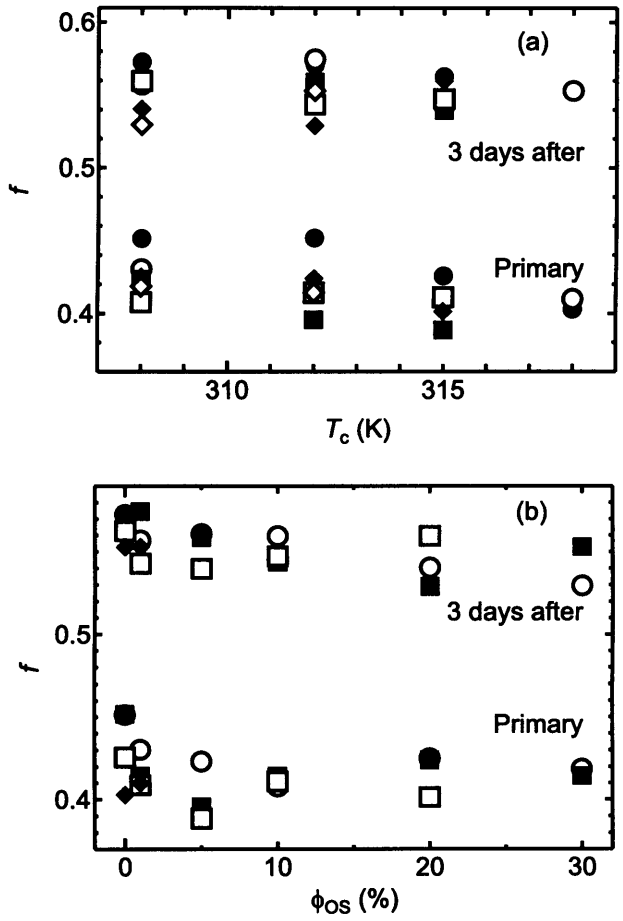

Figure 3.8: (a) Crystallization temperature and (b) OS content dependence of the fraction of the crystalline component in transverse relaxation signals at t_p and t_t. The symbols are identical to those in Fig. 3.6.

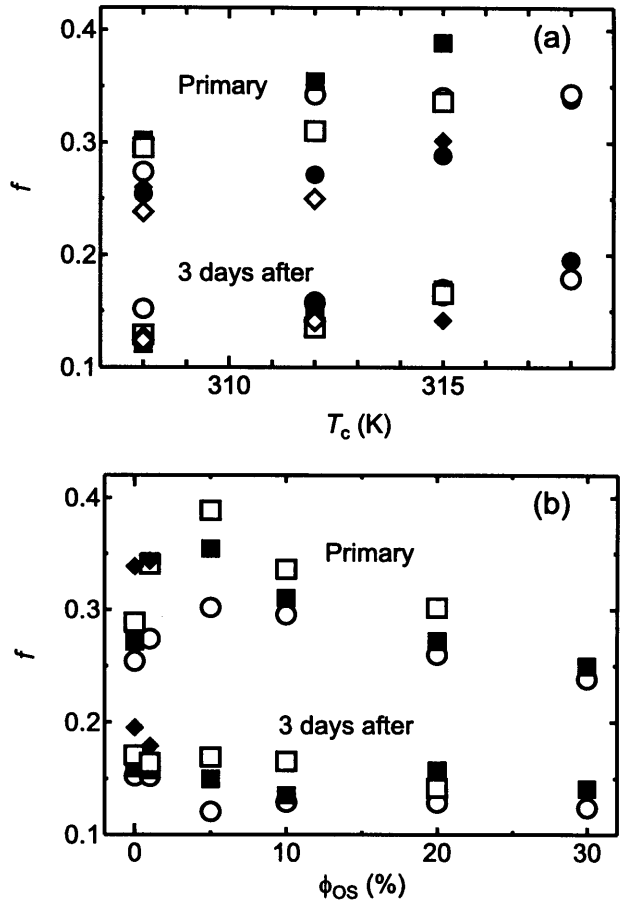

Figure 3.9: (a) Crystallization temperature and (b) OS content dependence of the fraction of the amorphous component in transverse relaxation signals both at t_p and t_t. The symbols are identical to those in Fig. 3.6.

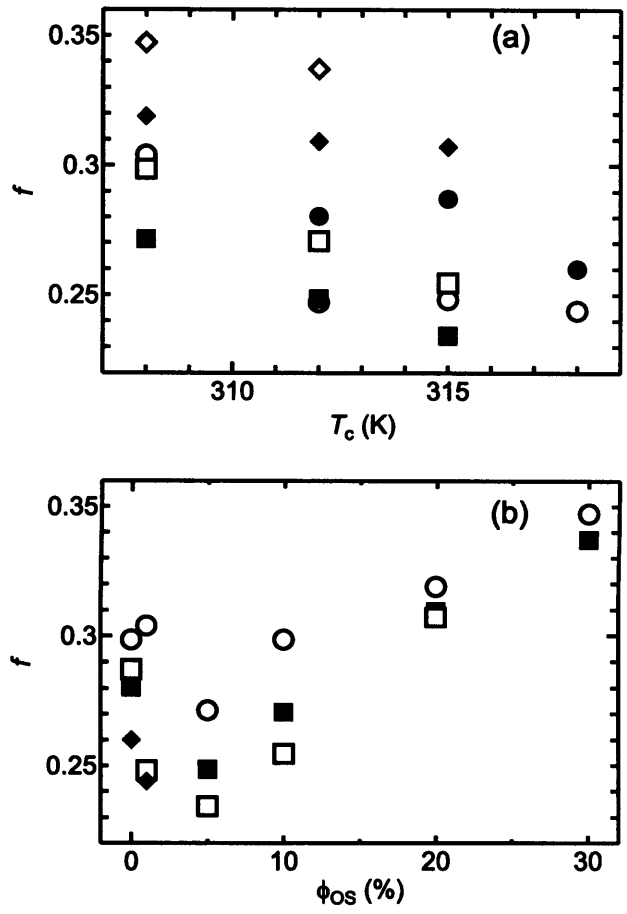

Figure 3.10: (a) Crystallization temperature and (b) OS content dependence of the fraction of the intermediate component in transverse relaxation signals at t_p. The symbols are identical to those in Fig. 3.6.

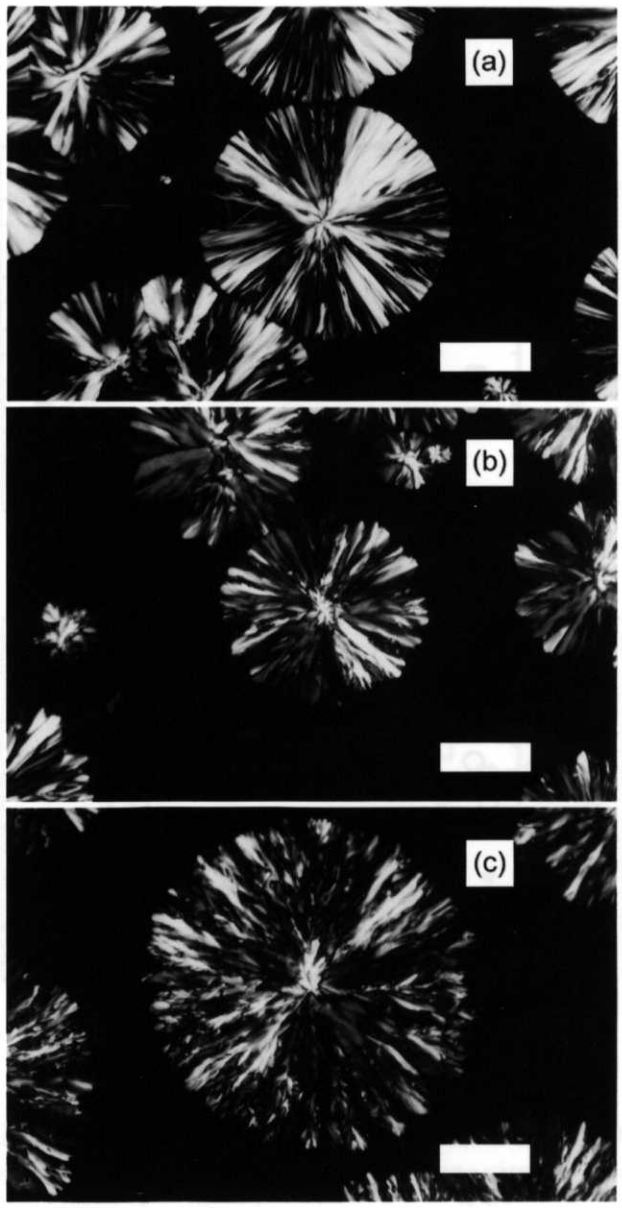

Figure 3.11: Polarized micrographs of spherulites of PCL blended with styrene oligomer. (a) $\phi_{OS} = 0\%$, $t = 20$ min, (b) $\phi_{OS} = 5\%$, $t = 21$ min. (c) $\phi_{OS} = 10\%$, $t = 43$ min. Bar 100 μm.

changes in these regions. The increase of f_c and the decrease of f_a and f_i in the secondary process is the consequence of the growth of the crystals which incorporate surrounding interfaces and amorphous chains. The value of T_2 for the crystalline component, on the other hand, is almost constant as discussed with Eq. 3.2 below.

The change of T_2 can be understood based on the theory of the line shape [20]. The magnetization $M(t)$ in the spin-spin relaxation process is described by

$$M(t) = M_0 \exp\left[-{\sigma_0}^2 {\tau_c}^2 \left\{\exp\left(-t/\tau_c\right) + t/\tau_c - 1\right\}\right], \tag{3.1}$$

where M_0 is the initial magnetization, ${\sigma_0}^2$ is the second moment of the resonance line of the rigid lattice, and τ_c is the correlation time of the fluctuating local field arising from surrounding spins. When mobility is small, i. e. $\sigma_0 \tau_c \gg 1$, as in crystals, Eq. 3.1 reduces to

$$M(t) = M_0 \exp\left[-\left(t/T_2\right)^2/2\right], \tag{3.2}$$

where $T_2 = {\sigma_0}^{-1}$. The value of T_2 is independent of molecular mobility at this limit. When mobility is large, i. e. $\sigma_0 \tau_c \ll 1$, it is expressed by

$$M(t) = M_0 \exp\left(-t/T_2\right), \tag{3.3}$$

where $T_2 = {\sigma_0}^{-2} {\tau_c}^{-1}$. Equation 3.2 describes the relaxation of the crystalline phase and Eq. 3.3 describes that of the intermediate and amorphous components.

The values of T_2 of the intermediate and amorphous components increase with T_c as shown in Fig. 3.6. This is explained by decreased τ_c by thermal motion. On the other hand, T_2 of the crystalline component is almost constant since the change of τ_c affects little to T_2 in a solid system.

The decrease of T_2 of the intermediate and amorphous components with increasing ϕ_{OS} (Fig. 3.6(b)) is the evidence that the OS rejected from crystals is mixed with PCL on the molecular level in amorphous regions and in interfaces for the following reasons. First, the value of T_2 is determined by the molecular mobility on a local spatial scale, which is usually less than of the order of 1 nm. Second, the mobility of pure OS is lower than that of amorphous PCL in the present experimental temperature range (Fig. 3.3). The decrease of T_2 in Fig. 3.6(b) shows the existence of the immobile protons of OS close to the mobile protons of PCL in amorphous and interfacial regions. The value of T_2 of the crystal, on the other hand, is independent of ϕ_{OS} though mixed OS may make the crystalline structure less perfect and decrease τ_c. This is because the situation in crystals is in the immobile limit as explained above by Eq. 3.2.

3.4.2 Changes of f

The structure of lamellar crystals is schematically shown in Fig. 3.12. In the work on pure PCL by pulsed NMR [11], the thickness of a crystal, an interface, and an amorphous layer of PCL was estimated to be 18 nm, 3 nm, and 9 nm, respectively, by assuming an ideal two-dimensional lamellar structure. Since two interfacial regions are on both sides of a lamellar crystal, the value of f_i is twice what is estimated from the thickness. This estimation is also applicable to the present data of pure PCL and gave almost the same values. For example, they were 18 nm, 5 nm, and 9 nm, respectively, for OS0 at $T_c = 315$ K.

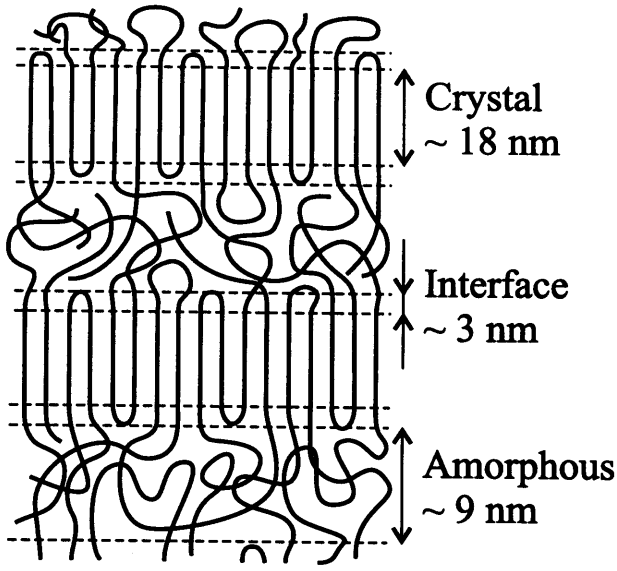

Figure 3.12: Schematic figure of lamella crystals showing crystalline, interfacial, and amorphous zones.

The value of f_c is the crystallinity based on the number of protons. It is easily converted into weight crystallinity $f_c^{(w)}$ with the ratios of the number of the protons in the repeating unit to its molecular weight of the constituent polymers. In the present system, the two crystallinities are almost the same ($f_c^{(w)} = 0.96 f_c$ at $\phi_{OS} = 30\%$ and $f_c^{(w)} = f_c$ at 0%).

The increase of f_c and the decrease of f_a with increasing T_c in Fig. 3.7 is ascribed to the polydispersity of PCL [21]. The molecules with lower molecular weight have less chance to crystallize at higher T_c; the amount of the crystallizable PCL decreases with increasing T_c. The decrease of f_i is the consequence of the more regular lamella-stack structure created at higher T_c through a slower crystallization rate. The fraction of the interface can be an index of regularity of the lamellar structure since it is a defect that does not exist in an ideal crystal.

The details of the behavior of f are displayed in Figs. 3.8–3.10. First, we look at the behavior of the crystal. Fig. 3.8 shows less dependence of f_c on T_c and ϕ_{OS} at t_t than at t_p. This implies that the secondary crystallization process has the effect of annealing. It diminished the differences in the crystallization conditions. The annealing effect appears in the amorphous component as well (Fig. 3.9). It also shows less dependence on T_c and ϕ_{OS} at t_t than at t_p. The maximum at $\phi_{OS} = 5\%$ at t_p is discussed later.

Next, we discuss the behavior of f_i based on the relation with the regularity of the lamellar structure mentioned above in the discussion of Fig. 3.7. Figure 3.10 shows that lower T_c and higher ϕ_{OS} results in a large value of f_i. On the other hand, the change of f_c must also be considered in discussions of f_i since interfacial layers always accompany a crystal; the amount of interfaces is dependent on that of crystals as well.

Figures 3.7, 3.8, and 3.10 show both f_c and f_i decreases with increasing T_c. These figures do not clearly show whether f_i really decreases or the decrease of f_i is a consequence of the decrease of f_c. When discussing the behavior of the interface, we have to consider

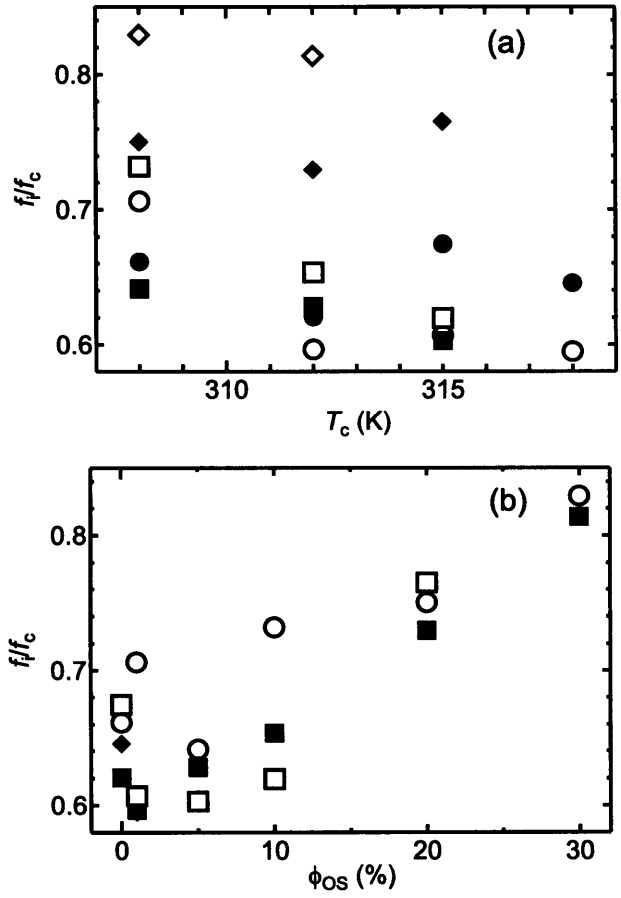

Figure 3.13: Plots of the ratio of f_i to f_c against (a) T_c and (b) ϕ_{OS} at t_p. The symbols are identical to those in Fig. 3.6.

the ratio f_i/f_c rather than f_c and f_i respectively to clarify the change of the interface. Figure 3.13(a) shows the plot of f_i/f_c against T_c at t_p. It enables us to confirm the decrease of f_i with increasing T_c. It indicates that the lamellar structure crystallized at higher temperature is more regular when the relation between the amount of the interface and regularity of the lamellar structure is considered as mentioned above.

The value of f_c was almost constant and f_i increased with ϕ_{OS} for $\phi_{OS} \gtrsim 5\%$ at t_p as shown in Figs. 3.8 and 3.10. The plot of f_i/f_c against ϕ_{OS} at t_p is shown in Figure 3.13(b), which indicates the increase with ϕ_{OS}. When ϕ_{OS} dependence of f_i/f_c is discussed, the contributions of OS in the interfaces must be taken into account. There are two reasons considered for the increase of f_i/f_c. One is the low regularity of the lamellar structure because of the existence of the impurities. The other is the contribution of rejected OS coexisting with PCL in interfaces on the molecular scale as discussed with the T_2 data (Fig. 3.6(b)). The present data do not show which factor is dominant in the PCL/OS systems. It requires more investigation to clarify the influences of ϕ_{OS} on f_i.

3.4.3 Secondary crystallization

To examine what happens in the secondary crystallization process, the ratio of f at t_t to that at t_p (f_t/f_p) was plotted against ϕ_{OS} in Fig. 3.14. The values of f_t/f_p of the crystalline and intermediate components have maxima at $\phi_{OS} \simeq 5\%$ and the amorphous component has a minimum at 5%.

The secondary crystallization is an ordering process in which the structures of melt crystallized polymers change to be closer to the ideal crystal with no defect such as interfaces or the lamellar stack structures. In this process, (i) lamellar thickening, (ii) lamella generation (crystallization in the interlamellar amorphous zones), and (iii) rejection of OS from the regions of the growing crystals occur. As indicated by Fig. 3.14(a) and (b), f_c increases ($f_t/f_p > 1$) and f_a decreases ($f_t/f_p < 1$) in the secondary process. The change of f_i varies according to the above three cases. In case (i), where existing crystals grow incorporating surrounding amorphous chains and interfaces, f_i decreases because of the effect of incorporation into the growing crystals. In case (ii), f_i must increase since new lamellar crystals and accompanying interfaces appear. In case (iii), part of the rejected OS must be trapped in interfaces as in the primary crystallization discussed with Fig. 3.6(b). This factor increases f_i. This process occurs both in cases (i) and (ii). The situations of cases (i)–(iii) are schematically illustrated in Fig. 3.15. The increase or decrease of f_i indicates which case is in progress in the secondary crystallization process.

The intermediate component shows $f_t/f_p > 1$ for $1 \lesssim \phi_{OS} \lesssim 20$ and $f_t/f_p < 1$ otherwise as indicated in Fig. 3.14(c). Since the plot shape is similar to that of f_c (Fig. 3.14(a)), the increase or decrease of f_i must be related to the amount of the crystals created in the secondary process. Cases (ii) and (iii) explain the change of the intermediate component since f_c and f_i show the same plot shape in these cases. On the contrary, f_t/f_p for the crystal and interface would show opposite plot shapes in case (i). However, lamellar thickening plays an important role at least in the regions where $f_t/f_p < 1$ for the interface. PCL lamellae are reported to thicken after about 10^3 s of crystallization time according to the study of the melting point [22]. On the other hand, x-ray scattering experiments showed that lamellae in PCL/PS do not thicken [16] and that the long period is almost

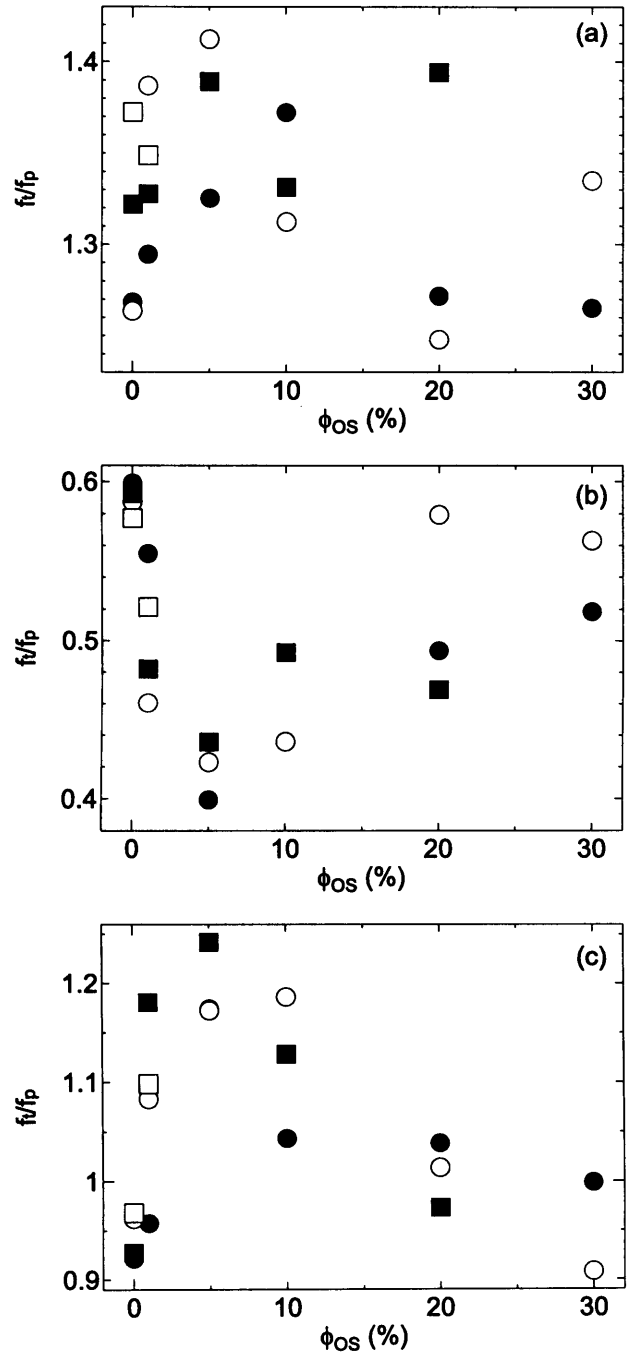

Figure 3.14: Styrene oligomer content dependence of the ratio of the fraction of each component at t_t to that at t_p. (a) crystalline, (b) amorphous, and (c) intermediate component. The symbols are identical to those in Fig. 3.6(b).

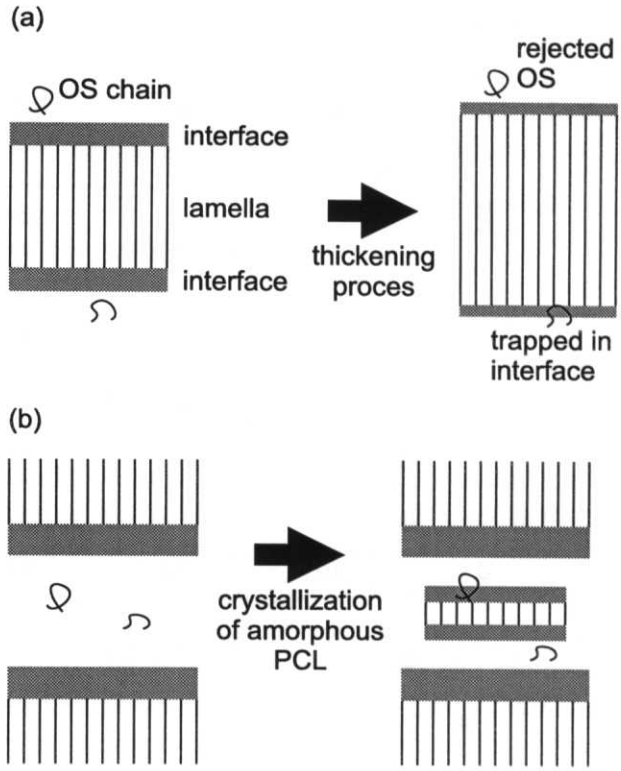

Figure 3.15: (a) Schematic figure of lamellar thickening process in which existing lamellae grow incorporating surrounding interfaces and amorphous chains. (b) Schematic figure of the crystallization in an interlamellar amorphous zone. The new lamella appears along with the interfaces.

constant [17] during the shorter crystallization periods of around 10^3 s.

The plot shape of the crystal in Fig. 3.14(a) is also similar to that of the amorphous component at t_p in Fig. 3.9(b). This indicates that the amount of the crystal increases more in the secondary process when a larger amount of amorphous chains is still left at t_p.

3.4.4 Rejection of impurities

According to Fig. 3.11, fibrillar spherulites start to be observed by optical microscopy at $\phi_{OS} \simeq 5\%$. During crystallization OS is rejected from crystals into three possible areas, namely interlamellar, interfibrillar, and interspherulitic zones [14]. Since optical micrography showed that spherulites of the blends fill the whole volume, the interspherulitic regions are ruled out as the destination of rejected OS. It is mainly interlamellar regions when the fibrillar structure is unclear ($\phi_{OS} \lesssim 5\%$). For $\phi_{OS} \gtrsim 5\%$, it must be rejected into both interlamellar and interfibrillar zones.

The PCL/OS blends with the present molecular weights undergo phase separation at $\phi_{OS} \simeq 40\%$ (Fig. 3.1). It may occur in the amorphous regions since the rejection of OS increases ϕ_{OS}. The values of ϕ_{OS} of the two phases after phase separation are about 40% and almost 100% according to the phase diagram.

The following two hypotheses are proposed here. One is that the change of the behavior at $\phi_{OS} = 5\%$ in Fig. 3.14 is ascribed to the change of morphology of spherulites. It explains the ϕ_{OS} dependence of f_c at t_p (Fig. 3.8(b)). For $\phi_{OS} \lesssim 5\%$, rejected OS increases the local value of ϕ_{OS} around growing crystals and lessens the amount of the crystals produced in the primary process. For $\phi_{OS} \gtrsim 5\%$, OS is additionally rejected into the interfibrillar zones. This effect slows down the increase of local ϕ_{OS}; the value of f_c at t_p is affected little by the blend composition. This relationship between morphology and the results of NMR, however, must be investigated farther to confirm its validity.

The second hypothesis is that ϕ_{OS} increased by the rejection of OS induces local phase separation in interlamellar amorphous regions. It can explain the change at 5% in Figs. 3.8(b) and 3.9(b) as follows: the composition of the OS-rich phase, which emerges with phase separation, is nearly OS 100%. Its T_2 is close to that of the crystalline state (Fig. 3.3). The NMR signal from the OS-rich phase is therefore superposed on the crystalline component since NMR in our experiments does not have enough resolution to decompose the two phases. As schematically indicated in Fig. 3.16, f_c increases and $f_a$decreases approximately by the amount of the emerging OS-rich phase.

The condition that phase separation takes place is expressed by

$$\phi_{OS}^{(res)} = \phi_{OS}/(1-\theta) > \phi_b, \tag{3.4}$$

where $\phi_{OS}^{(res)}$ is the local blend composition in the residual amorphous regions after crystallization, θ is weight crystallinity ($0 < \theta < 1$), and ϕ_b is the binodal composition ($\simeq 40\%$) shown in the phase diagram. The value of θ is calculated from the value of the dashed line in Fig. 3.16(a), which is the crystallinity based on the number of protons. The condition of Eq. 3.4 is met only for $\phi_{OS} \gtrsim 30\%$ with the values of ϕ_{OS}, θ, and ϕ_b in the present experiments. The calculated value of $\phi_{OS}^{(res)}$, however, is an average in the whole sample. There is a possibility that the local value of $\phi_{OS}^{(res)}$ around lamellae is different and that

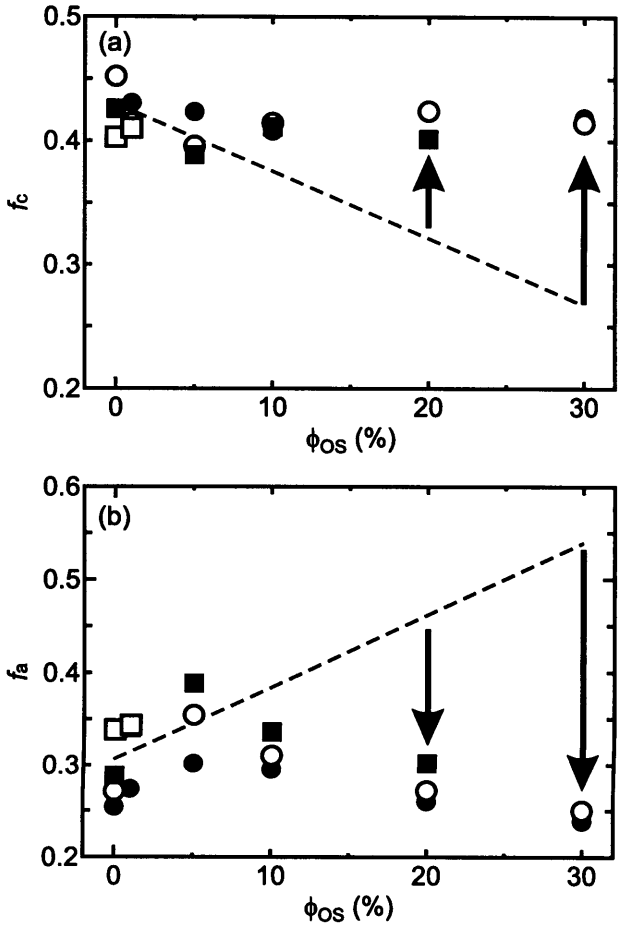

Figure 3.16: Schematic illustration that explains the changes of (a) f_c and (b) f_a at t_p induced by phase separation.

phase separation really takes place on a microscopic scale. This hypothesis also requires more investigation.

3.5 Conclusions

The crystallization process of PCL/OS blends was investigated by measuring the transverse relaxation by pulsed NMR. The decrease of T_2 of the intermediate and amorphous components with increasing ϕ_{OS} indicated that OS is rejected into the residual amorphous PCL and the interfaces during crystallization. The decrease of f_c with increasing T_c is ascribed to the polydispersity of PCL. The values of f_c and f_a depended less on T_c and ϕ_{OS} after the secondary crystallization proceeded than at the end of the primary process. This indicates that the secondary crystallization has the effect of annealing. The value of f_i can be an index of regularity of the lamellar structure. Its change implied which process of lamellar thickening, lamella generation, and the rejection of OS was dominant in the secondary crystallization. We also discussed which region OS was rejected into. The changes of f in the secondary process showed extreme values at $\phi_{OS} \simeq 5\%$. We proposed two hypotheses to discuss this behavior. One is the influence of the morphology of the spherulites. The structural change at 5% into the fibrillar spherulites and the additional exclusion of the impurities into interfibrillar zones may explain it. The other is the possibility of local phase separation during crystallization. The increased value of ϕ_{OS} in the interlamellar regions induces phase separation on a small scale. It produces a phase whose ϕ_{OS} is almost 100%. The values of f_c and f_a change by the amount of it.

References

[1] L. Mandelkern, "Crystallization of Polymers", New York, McGraw-Hill, (1964).

[2] B. Wunderlich, "Macromolecular Physics", vol. 2, New York, Academic Press, (1980).

[3] R. A. Fava ed., "Method of Experimental Physics", vol. 16, Polymers Part B, Crystal Structure and Morphology, New York, Academic Press, (1980).

[4] D. R. Paul, J. W. Barlow, in D. Klempner and K. C. Frisch eds., "Polymer Alloys II", New York, Plenum, (1980).

[5] L. A. Utracki, "Polymer Alloys and Blends", Munich, Vienna, New York, Hanser, 1989.

[6] K. Fujimoto, T. Nishi, and R. Kado, Polym. J., **3**, 448 (1972).

[7] R. Kitamaru, F. Horii, S.-H. Hyon, J. Polym. Sci., Polym. Phys. Ed., **15**, 821 (1977).

[8] V. J. McBrierty and D. C. Douglass, J. Polym. Sci. Macromol. Rev. **16**, 295 (1981).

[9] V. J. McBrierty and D. C Douglass, Phys. Rept., **63**, 63 (1980).

[10] D. C. Douglass and V. J. McBrierty, and T. A. Weber, J. Chem. Phys., **64**, 1533 (1976).

[11] H. Tanaka and T. Nishi, J. Appl. Phys., **59**, 1488 (1986).

[12] H. Tanaka and T. Nishi, J. Chem. Phys., **85**, 6197 (1986).

[13] T. Ikehara and T. Nishi, Act. Polym., **46**, 419 (1995).

[14] R. S. Stein, F. B. Khambatta, F. P. Warner, T. Russell, A. Escala, and E. Balizer, J. Polym. Sci., Polym. Symp., **63**, 313 (1978).

[15] H. Tanaka and T. Nishi, Phys. Rev. A, **39**, 783 (1989).

[16] Y. Li and B. J. Jungnickel, Polymer, **34**, 9 (1993).

[17] S. Nojima, K. Kato, M. Ono, and T. Ashida, Macromolecules, **25**, 1922 (1992).

[18] S. Nojima, K. Satoh, and T. Ashida, Macromolecules, **24**, 942 (1991).

[19] J. D. Hoffman and J. J. Weeks, J. Res. Nat. Bur. Stand., **66A**, 13 (1962).

[20] R. Kubo and K. Tomita, J. Phys. Soc. Jpn., **9**, 888 (1954).

[21] F. Gornick and L. Mandelkern, J. Appl. Phys., **33**, 907 (1962).

[22] P. J. Phillips and G. J. Rensch, J. Polym. Sci., B, Polym. Phys., **27**, 155 (1989).

Chapter 4

Interpenetrated spherulites

4.1 Introduction

Poly(butylene succinate)/poly(vinylidene chloride-*co*-vinyl chloride) (PBSU/PVDCVC) blends are a miscible crystalline/crystalline polymer system above the melting points. They were found to show interpenetrated (or interlocked) spherulites [1], which do not stop growing when they collide with neighboring spherulites. An important factor to realize interpenetration is the simultaneous growth of the spherulites of the two constituents. The melting points T_m of PBSU and PVDCVC are 387 K and 421 K, respectively. On the other hand, the spherulitic growth rate G of PBSU, the lower-T_m component, is usually faster than that of PVDCVC, the higher-T_m component. This enables the crystallization of the lower-T_m component to influence that of the higher-T_m component in this system. PBSU/PVDCVC blends were discovered in a series of studies of polyester/poly(vinylidene halide) systems by our group [1–3].

Studies of miscible pairs of crystalline polymers with different chemical structures [4–9] are still restricted compared with crystalline/amorphous and amorphous/amorphous blends. The reported T_m differences are usually about 100 K in these systems. The higher-T_m component crystallizes first in the crystallization process and the other component crystallizes in the crystals where it is specially constrained. Hence, the simultaneous growth of the spherulites of both components is hardly observed except the blends of the same kind of polymers such as low-density and high-density polyethylene. Our group has been seeking crystalline/crystalline polymer blends with different chemical structures exhibiting simultaneous spherulitic growth.

The purpose of the present paper is to investigate the dependence of G on the crystallization temperature T_c, the conditions of the formation of interpenetrated spherulites, and their morphology by optical microscopy.

4.2 Experimental

The characteristics of the samples are displayed in Table 4.1. The constituent polymers were dissolved into a mutual solvent N,N-dimethylformamide at about 370 K. Cast films were prepared on glass plates and they were dried in air before the removal of the residual

solvent in a vacuum chamber for several days at room temperature. They were covered by other glass plates for optical microscopy.

Table 4.1: The characteristics of the samples: source, weight average molecular weight M_w, glass transition temperature T_g, and melting temperature T_m.

Sample	Source	M_w	T_g (K)	T_m (K)
PBSU	Showa Denko	140,000	241	387
PVDCVC*	Asahi Chemical	100,000	279	421

*vinylidene chloride/vinyl chloride = 80/20.

The spherulitic growth was observed under crossed nicols with a polarizing microscope (Olympus BHA-P) and a temperature controller (Linkam LK-600PM). After melted at 443 K for 10 min, the samples were quenched to T_c at -100 K/min. A test plate of 530 nm was used if necessary since small birefringence of PVDCVC makes optical microscopic observation difficult. The compositions of the blends were PBSU/PVDCVC (wt/wt) = 30/70, 40/60, 50/50, and 60/40. The experimental temperature range was 338 K $\leq T_c \leq$ 378 K at intervals of 5 K.

4.3 Results

As shown in Fig. 4.1 neat PBSU showed bright, negative spherulites, and PVDCVC showed dark, positive spherulites. These differences make distinguishing the spherulites of the two polymers easy by optical microscopy. Table 4.2 summarizes the results of the spherulitic growth. Interpenetrated spherulites were observed under all the conditions where both constituents showed spherulitic growth. It should be noted that the spherulites of neat PBSU or PVDCVC never showed interpenetration by themselves.

Table 4.2: The conditions for spherulitic growth. ⊗: both PBSU and PVDCVC showed spherulitic growth. ○: only PBSU spherulites were observed. ×: only PVDCVC spherulites grew. −: no experiments were performed.

	T_c (K)								
PBSU/PVDCVC	338	343	348	353	358	363	368	373	378
30/70	⊗	⊗	⊗	⊗	×	×	−	−	−
40/60	○	○	⊗	⊗	⊗	⊗	×	−	−
50/50	−	−	⊗	⊗	⊗	⊗	⊗	⊗	−
60/40	−	−	−	○	○	⊗	⊗	⊗	×

Figure 4.2 shows the T_c dependence of G. Spherulites grew linearly until they collided with neighboring ones as in the previous work [1]. PBSU and PVDCVC had almost the same values of G in a 30/70 blend. They were approximately the same at about 360 K,

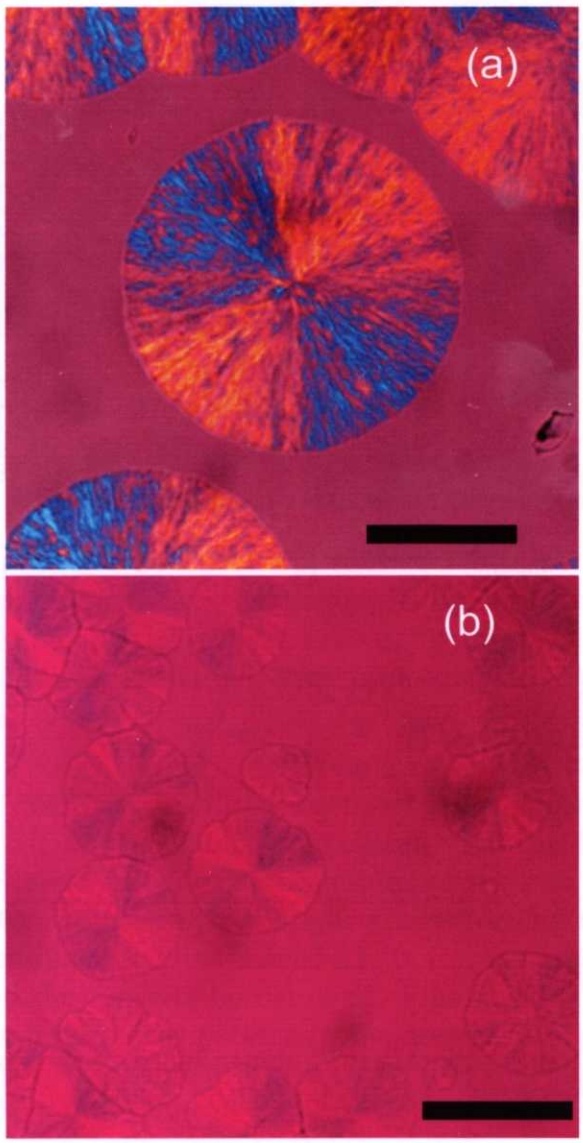

Figure 4.1: Spherulites of (a) PBSU crystallized at 363 K and (b) PVDCVC at 358 K, which show negative and positive spherulites, respectively. Bar 50 μm.

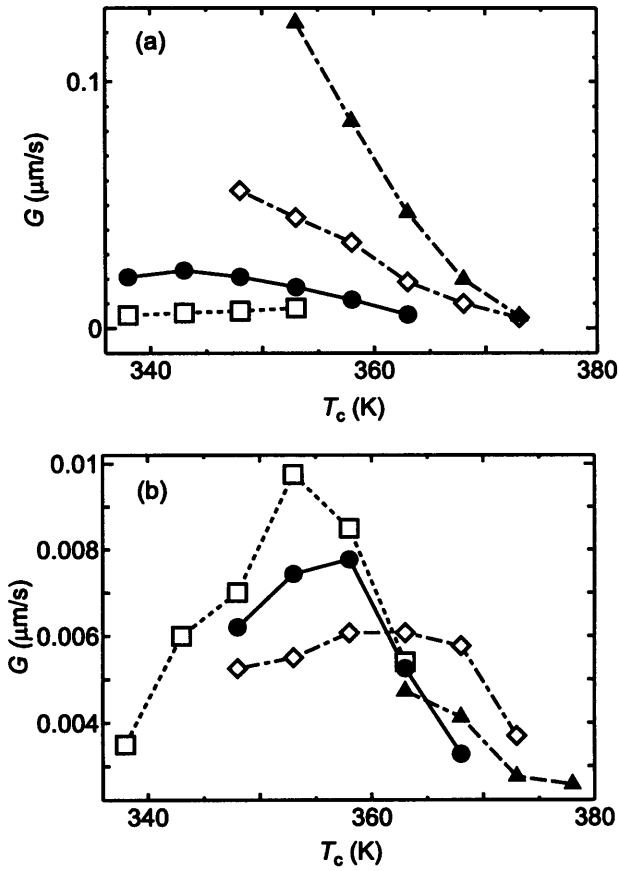

Figure 4.2: Crystallization temperature T_c dependence of the spherulitic growth rate G of (a) PBSU and (b) PVDCVC. PBSU/PVDCVC = 30/70 (□), 40/60 (•), 50/50 (◇), and 60/40 (▲).

370 K, and 370 K for 40/60, 50/50, and 60/40 blends, respectively. The blend composition influenced G of PBSU, whereas it affected little that of PVDCVC. The peak temperature of G of PVDCVC increased with the PBSU content, and the G-T_c lines crossed around 360 K.

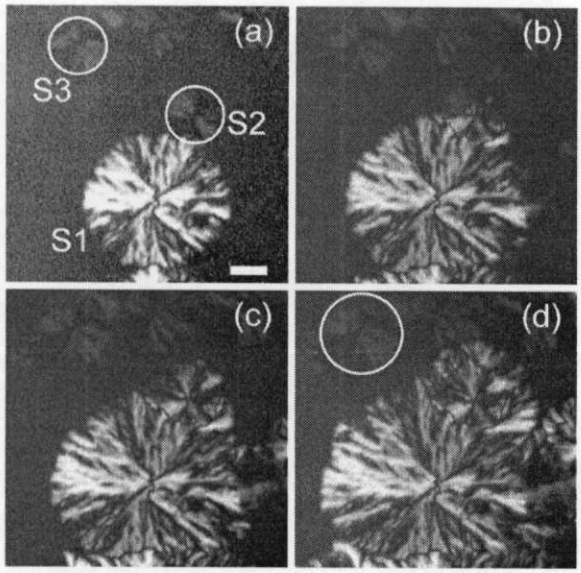

Figure 4.3: The process of interpenetration in a 40/60 blend at 353 K. The crystallization times are (a) 44 min, (b) 55 min, (c) 60 min, and (d) 70 min. The white lines indicate the positions of PVDCVC spherulites. S1 is a PBSU spherulite and S2 and S3 are PVDCVC spherulites. Bar 10 μm.

The penetration process, which will be discussed later, is displayed in Fig. 4.3. The bright spherulite of PBSU at the center (S1) collided with the dark spherulite of PVDCVC (S2) on the upper right in (a). The brightness of the area in S2 near the collision border gradually increased in (b) and the bright area expanded toward the center of S2. At the same time, S1 continued to grow around S2. In (c), the bright area in S2 passed the center of S2 and reached the opposite border of S2. Finally, in (d), S1 surrounded S2 and continued to grow. The birefringent pattern in the area of S2 was not the superposition of S1 and S2 after the penetration; the apparent pattern was that of a PBSU spherulite whose center is located at the center of S2. In Fig. 4.3(a), the size of S2 was the same as that of the PVDCVC spherulite close to the upper left corner of the photograph (S3). After S1 passed S2 in (d), the size of S2 was almost unchanged while S3 continued to grow.

PBSU spherulites showed three birefringent patterns under crossed nicols with a test plate according to the crystallization conditions as in Fig. 4.4: (a) negative spherulites, (b) disordered near the center and negative in the outer regions, and (c) neither negative nor positive spherulites that rotated by about 45° from the positive and negative patterns. The change of the birefringent pattern is summarized in Fig. 4.5.

As exhibited in Fig. 4.6, the birefringent pattern in penetrated PVDCVC spherulites was close to that of PBSU. The birefringent patterns of PBSU and PVDCVC spherulites

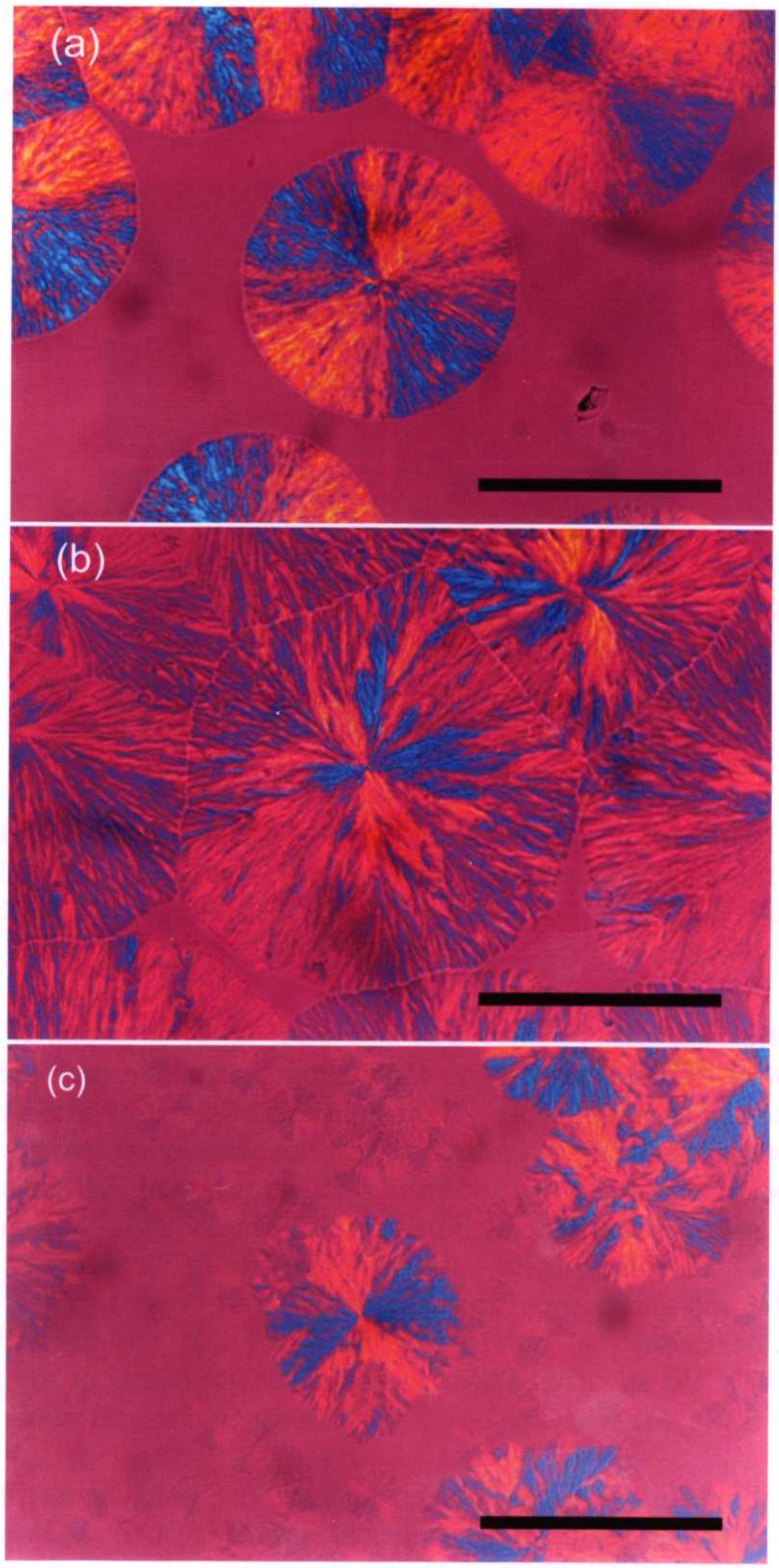

Figure 4.4: Birefringent patterns of PBSU spherulites. (a) Negative spherulites of neat PBSU crystallized at 368 K for 6 min. (b) A 60/40 blend crystallized at 358 K for 35 min. (c) A 50/50 blend crystallized at 363 K for 72 min. Bar 100 μm.

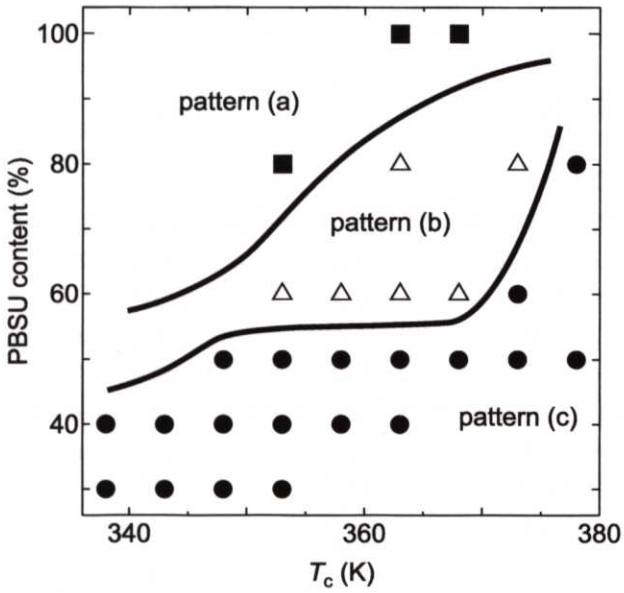

Figure 4.5: Dependence of the birefringent patterns of PBSU spherulites on T_c and the PBSU content. ■: pattern (a), △ : pattern (b), and •: pattern (c) in Fig. 4.4.

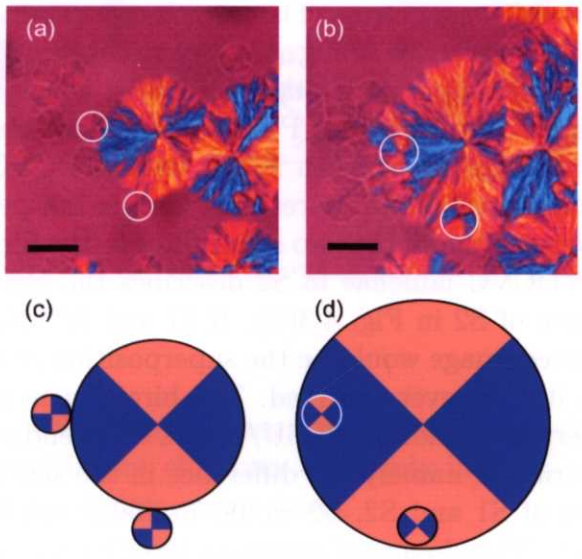

Figure 4.6: Penetration process of a PBSU spherulite of pattern (c) in Fig. 4.4 for PBSU/PVDCVC = 50/50 crystallized at 363 K for (a) 45 min and (b) 65 min. The white lines indicate the positions of PVDCVC spherulites. (c) and (d) are the schematic figures of (a) and (b), respectively. Bar 20 μm.

were pattern (c) and positive, respectively, before penetration. After penetration, the area of PVDCVC spherulites showed similar birefringence as PBSU.

4.4 Discussions

As indicated in Fig. 4.1, the spherulites of PVDCVC were darker than those of PBSU under crossed nicols. It shows that PBSU has larger birefringence than PVDCVC. The possible causes for this result are the differences of the thickness of the sample, the crystalline structure, the lamellar thickness, and the density of lamellae. The thickness of the sample is ruled out since it is almost the same for the spherulites of the two components growing simultaneously in blended samples. Though quantitative estimation of the film thickness was not performed, the film thickness must have been thin enough for the spherulites to contact with both upper and lower glass plates in all the photographs in this paper and to grow two-dimensionally.

The spherulitic growth of the two components was observed under almost all experimental conditions as shown in Table 4.2. The induction periods until the onset of primary nucleation, however, were different for the two specimens. PBSU generally appeared first at the lower experimental temperature range and vice versa at the higher range. Nonetheless, the two components show simultaneous spherulitic growth in any case under almost all the present experimental conditions. After the spherulites of one component emerge, the increase of the concentration of the other specimen in the residual melt suppresses the crystallization of it. Though this possibly explains the complex T_c dependence of G of PVDCVC in Fig. 4.2, the details are still under study.

Interpenetration is now discussed here. The microscopic results showed that the area of S2 became brighter from the lower left in Fig. 4.3(a)–(c) and that the apparent birefringent pattern in S2 was almost the same with that of a PBSU spherulite in Fig. 4.3(d). The increase of brightness in S2 indicates that PBSU also crystallizes in this area when the difference in intrinsic birefringence between PBSU and PVDCVC is taken into account. Two possibilities are considered for these results. One is the penetration of S1 into S2 and the other is the superposition of the two spherulites in the film. Penetration of PBSU lamellae of S1 along PVDCVC lamellae in S2 describes the obtained results, especially the apparent birefringence of S2 in Fig. 4.3(d). If S1 and S2 merely superposed on each other in a film, the observed image would be the superposition of the birefringent patterns of S1 and S2. However, it was never observed. The birefringent pattern in S2 in Fig. 4.3 therefore proves the interpenetration in PBSU/PVDCVC blends. The termination of the growth of S2 after penetration, namely the difference in the size between S2 and S3, also denies the superposition of S1 and S2; S2 would probably continue to grow as S3 if it were superposed with S1. The change of apparent birefringence of PVDCVC in Fig. 4.6 also indicates the penetration of the lamellae of PBSU along those of PVDCVC.

The results show that PBSU penetrates into PVDCVC and that PVDCVC does not penetrate into PBSU. This can be explained by assuming the low density of lamellae in PVDCVC spherulites. The low density causes the observed low birefringence of the PVDCVC spherulites. Since PVDCVC is a copolymer, its crystallinity is low as indicated by small DSC melting peaks [1]. The situation of penetration is schematically illustrated in Fig. 4.7. Since the spherulites fill the whole space in these blends, the residual amor-

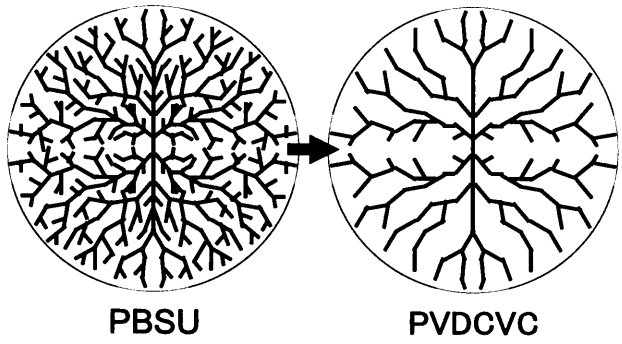

Figure 4.7: Schematic figure of the lamellar densities in PBSU and PVDCVC spherulites.

phous substances of the constituents stay inside the spherulites, namely interlamellar and interfibrillar regions. The sparse spherulites of PVDCVC contain a sufficient amount of amorphous PBSU. This enables the PBSU spherulite to penetrate into PVDCVC spherulites. To confirm the difference in the lamellar density, we applied atomic force microscopy to the present system. It showed the direct evidences for the difference in lamellar density of the two specimens. The detailed results will be published soon [10].

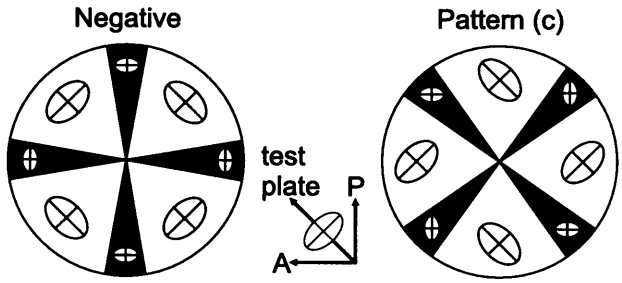

Figure 4.8: Schematic figure of the birefringent ellipsoids of PBSU in a negative spherulite and pattern (c) in Fig. 4.4.

Figure 4.4(c) shows PBSU spherulites that is neither positive nor negative. This pattern indicates the birefringent ellipsoids uniformly incline as shown in Fig. 4.8. The reason for this phenomenon is now under study.

Here, the present results are compared with the previous results [1] where M_w of PBSU was lower, 54,000. In the previous study, interpenetrated spherulites were observed only under restricted conditions, PBSU/PVDCVC $\simeq$ 40/60 and $T_c \simeq$ 360 K. They were observed, however, under almost all the experimental conditions in the present study as shown in Table 4.2. This disagreement is ascribed to the difference in G of PBSU. The value of G in the present work was slower; for instance, it was about a tenth of what was reported in the previous study for PBSU/PVDCVC $\simeq$ 40/60 and $T_c \simeq$ 350 K. The M_w dependence of G of PBSU is an interesting issue and requires more investigation.

References

[1] J.-C. Lee, H. Tazawa, T. Ikehara, and T. Nishi, Polym. J., **30**, 780 (1998).

[2] J.-C. Lee, H. Tazawa, T. Ikehara, and T. Nishi, J. Appl. Poly. Sci., B, Polym. Phys., **35**, 2645 (1997).

[3] J.-C. Lee, H. Tazawa, T. Ikehara, and T. Nishi, Polym. J., **30**, 327 (1998).

[4] J. P. Penning and R. St. John Manley, Macromolecules, **29**, 77 (1996).

[5] J. P. Penning and R. St. John Manley, Macromolecules, **29**, 84 (1996).

[6] K. Fujita and T. Kyu, *Macromolecules*, **29**, 91 (1996).

[7] M. Aubin, Y. Bedard, M. F. Morrissette, and R. E. Prud'homme, J. Polym. Sci., B, Polym. Phys., **21**, 233 (1983).

[8] H. Zhang, and R. E. Prud'homme, J. Polym. Sci., B, Polym. Sci., **24**, 723 (1987).

[9] M. Avella and E. Martuscelli, Polymer, **29**, 1731 (1988).

[10] Y. Terada, T. Ikehara, and T. Nishi, Polym. J., **32**, 900 (2000).

Part III

Dynamics of Miscible Polymer Blends

Chapter 5

Molecular mobility in miscible polymer blends

5.1 Introduction

Miscible amorphous/amorphous polymer blends are characterized by the mixed state of the constituents on the molecular level. Transparency of miscible blends, for instance, results from the homogeneous reflective index in the sample on the scale of the wavelength of visible light. Since they exhibit a single glass transition temperature T_g, the constituents are usually considered to have the same molecular mobility.

Polystyrene/poly(vinyl methyl ether) (PS/PVME) blends are amorphous/amorphous polymer blends with a phase diagram of the lower critical solution temperature (LCST) type. The system is in the homogeneous mixed phase under the critical temperature, about 410 K.

Only a few works report the application of pulsed NMR to these blends by measuring the spin-lattice relaxation time T_1 and the spin-spin relaxation time T_2 [1, 2]. The transverse relaxation in the mixed state was decomposed into two components, and the possibility of microscopic phase separation was proposed [1]. However, the detailed investigations of miscible polymer blends by pulsed NMR is still insufficient.

The relaxation times widely measured by pulsed NMR are T_1, T_2, and the spin-lattice relaxation time in the rotating frame $T_{1\rho}$. The relaxation curves are decomposed when a sample contains heterogeneous phases with different molecular mobility. The information on the heterogeneous domains smaller than the order of 10 nm and 1 nm is lost in T_1 and $T_{1\rho}$ measurements, respectively, because of spin diffusion [3]. The T_2 measurement is generally considered capable of obtaining the information on the heterogeneous domains smaller than the order of 1 nm. The heterogeneity in a system is estimated by measuring these three relaxation times.

The aim of the present paper is to apply ^{1}H pulsed NMR to miscible blends of PS/PVME and to investigate molecular mobility and miscibility with T_1, $T_{1\rho}$, and T_2. They are interpreted with the relaxation mechanism of nuclear magnetization.

5.2 Experimental

The samples were PS (M_w = 37900, M_w/M_n = 1.01, Tosoh) and PVME (M_n = 46500, M_w = 99000, Science Polymer Products). They were dissolved in a mutual solvent, toluene. The blends were dried in air at room temperature for two days before further removal of the solvent in a vacuum chamber at an elevated temperature between T_g and the critical temperature of phase separation for about a week. They were placed in NMR sample tubes, which were then filled with nitrogen gas and sealed. The phase diagram is displayed in Fig. 5.1.

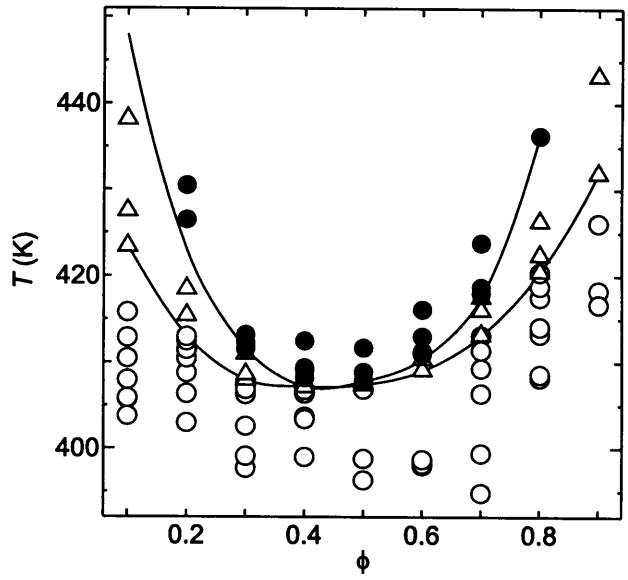

Figure 5.1: The phase diagram (temperature T vs. the PS content ϕ) of the PS/PVME blends showing binodal and spinodal points. The lines are the guide for the eye. ○: miscible, △: nucleation and growth, and •: spinodal decomposition.

Differential scanning calorimetry (DSC) measurements to obtain T_g were performed with TA Instruments DSC2920. The NMR equipment was Bruker PC-20 with the ^{1}H resonant frequency 20 MHz. The inversion recovery and solid echo pulse sequences were used for T_1 and T_2 measurements, respectively. The solid echo train pulse sequence was employed to measure $T_{1\rho}^*$, and $\lim_{\tau\to 0} T_{1\rho}^* = T_{1\rho}$ [4]. The repetition time of the 90° pulses τ was 5 μs. The experimental temperature was 318 K.

The obtained relaxation signals were analyzed by nonlinear least-square fitting method. The T_1 and $T_{1\rho}$ decay curves were fitted with exponential curves. The decay of magnetization with time t in transverse relaxation is practically fitted to the Gaussian $M_0 \exp\left[-(t/T_2)^2/2\right]$ and exponential $M_0 \exp(-t/T_2)$ functions for immobile and mobile systems, respectively, where M_0 is the amplitude. The transverse decay of the blends was decomposed into two components except for the samples with the high content of PS.

5.3 Results

The change of T_g with the PS content ϕ obtained by DSC is displayed in Fig. 5.2. All the blends showed one T_g. These results show that the blends are miscible. Transparency of the samples also indicated miscibility.

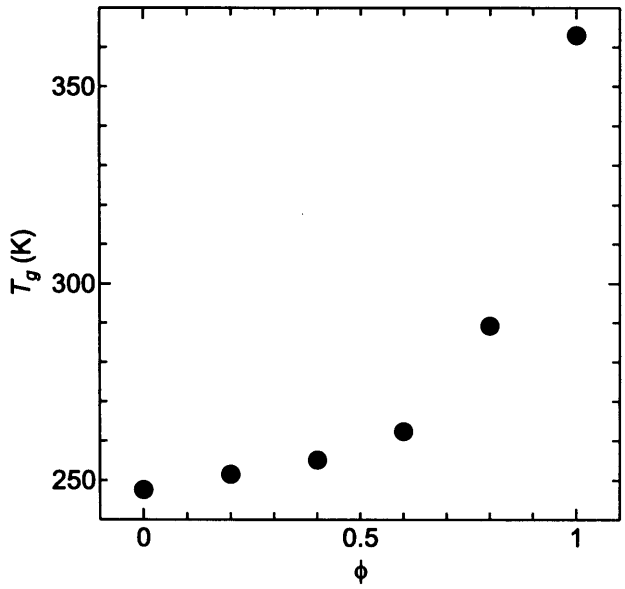

Figure 5.2: The glass transition temperatures T_g of the PS/PVME blends plotted against the PS content ϕ.

The results of the fitting analysis of pulsed NMR experiments are shown in Figs. 5.3, 5.4, and 5.5. The T_1 and $T_{1\rho}$ decay of all the samples contained one exponentially decaying component. Most transverse relaxation signals were decomposed into two components. The components with short and long T_2 showed Gaussian and exponential relaxation functions, respectively. The fractional amount f of the component with short T_2 is displayed in Fig. 5.5(b) along with the fraction of the number of the protons of PS f_p. The values of f were almost identical to f_p. The relaxation signals of the samples with high ϕ were fitted to only one Gaussian component. This is probably ascribed to the close relaxation times of the two components, which are difficult to be numerically decomposed.

5.4 Discussions

The experimental results indicating the homogeneity of the blends were transparency, single T_g, T_1, and $T_{1\rho}$. Transparency indicated homogeneity on the scale of the wavelength of visible light, and T_1 and $T_{1\rho}$ showed homogeneity on the spatial scale larger than the order of 1 nm. The spin-spin relaxations with two components, on the other hand, implied heterogeneity smaller than the order of 1 nm in the blends.

Two possibilities are proposed to interpret the NMR results. One is the phase separation on a spatial scale smaller than the order of 1 nm (model I). In this case, the two

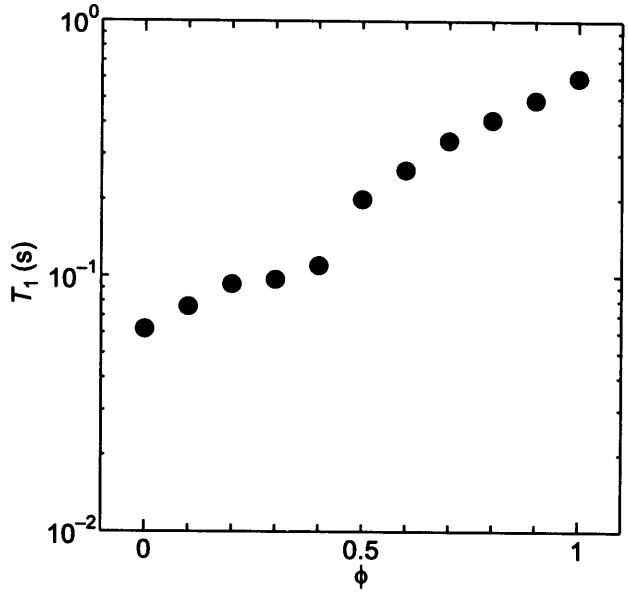

Figure 5.3: Dependence of the spin-lattice relaxation time T_1 on the PS content ϕ.

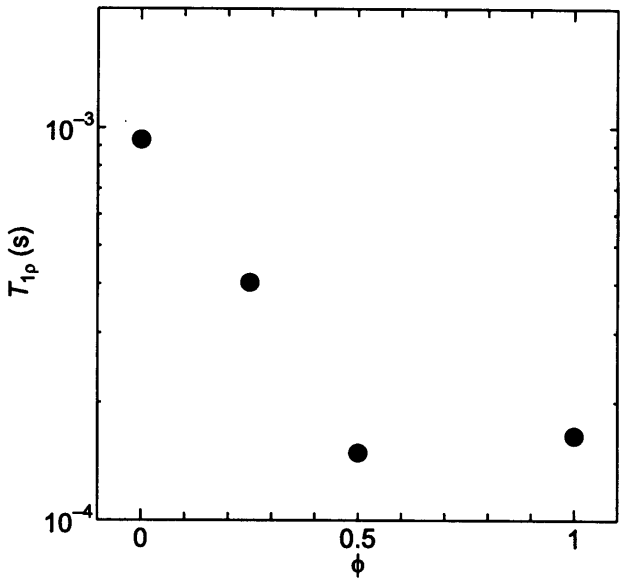

Figure 5.4: Dependence of the spin-lattice relaxation time in the rotating frame $T_{1\rho}$ on the PS content ϕ.

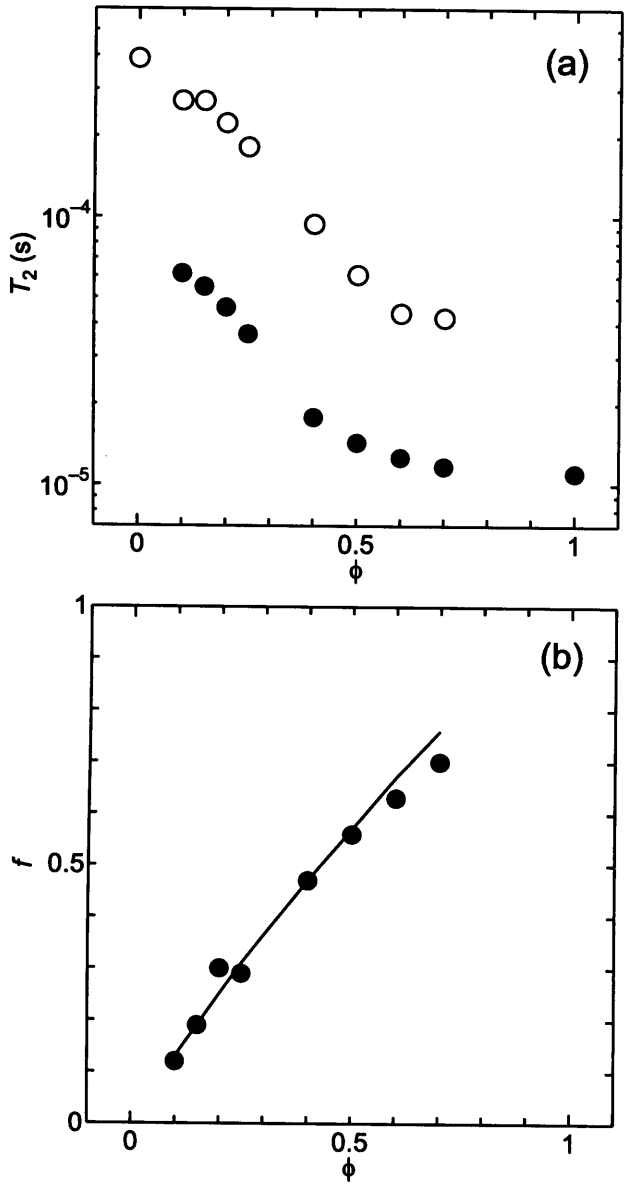

Figure 5.5: Dependence of (a) the spin-spin relaxation time T_2 and (b) the fractional amount f of the two components on ϕ. In (b), the line of the fractional amount of the number of protons of PS f_p is drawn.

components in transverse relaxation are assigned to the two microscopic demixed phases. The other possibility is the difference in molecular mobility between the two specimens mixed on the molecular level (model II).

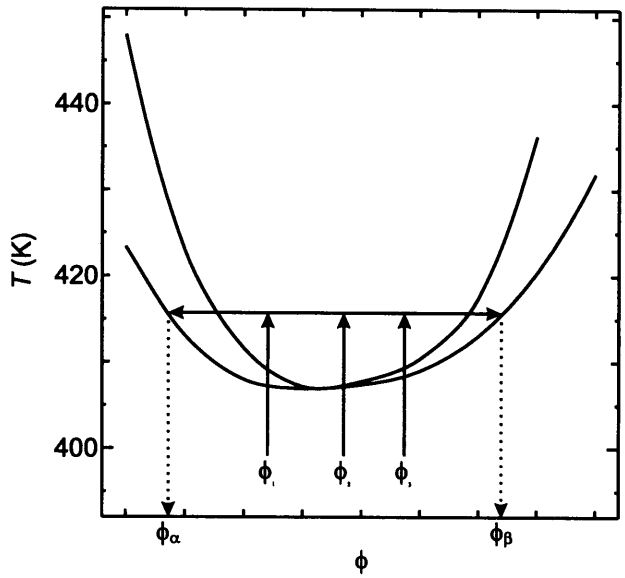

Figure 5.6: Schematic figure of the phase diagram showing macroscopic phase separation. The values of ϕ in the two demixed phases are ϕ_α and ϕ_β regardless of the initial value of the blends (ϕ_1–ϕ_3).

First, model I is discussed. Although this model may be widely accepted, it leads to conclusions inconsistent with two experimental results. One is the continuous change of T_2 with ϕ in Fig. 5.5(a). If microscopic demixed domains were formed by the identical mechanism to the macroscopic phase separation, the composition in the heterogeneous domains would be independent of ϕ (Fig. 5.6). In this case, T_2 is also independent of ϕ. The second one is the agreement between f and f_p in Fig. 5.5(b). It indicates the two components in the transverse relaxation are assigned to the protons of PS and PVME. If the microscopic demixed domains existed in the samples and if the two components of T_2 were attributable to the two phases, f and f_p would not be identical.

Next, the difference in molecular mobility in miscible polymer blends of model II is discussed. The relaxation time T_2 of a spin interacting with another identical spin by dipolar coupling is expressed by [5]

$$\frac{1}{T_2} = \frac{1}{5}\frac{\gamma^4\hbar^2}{r^6} I(I+1)\left[3\tau_c + \frac{5\tau_c}{1+\omega_0{}^2\tau_c{}^2} + \frac{2\tau_c}{1+4\omega_0{}^2\tau_c{}^2}\right], \tag{5.1}$$

where γ is the gyromagnetic ratio, $\hbar = h/2\pi$ where h is the Plank constant, I is the spin quantum number, ω_0 is the resonant frequency, and r is the distance between the interacting spins. Here, random molecular rotation is assumed and τ_c is the correlation time of motion. When multiple protons have dipole-dipole interactions, T_2 is expressed

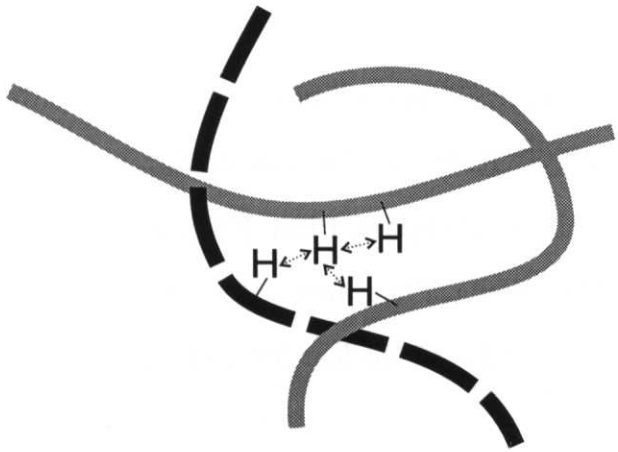

Figure 5.7: Schematic figure of dipolar interaction of protons. The thick dashed line and the solid shaded lines represent polymer molecules of the two different constituents. The thin dotted arrows denote the intramolecular and intermolecular dipolar interactions of protons.

by adding up the contributions of the interacting protons as

$$\frac{1}{T_2} = \frac{\gamma^4 \hbar^2 I(I+1)}{5} \sum_k {r_k}^{-6} \left[3\tau_{c(k)} + \frac{5\tau_{c(k)}}{1+{\omega_0}^2{\tau_{c(k)}}^2} + \frac{2\tau_{c(k)}}{1+4{\omega_0}^2{\tau_{c(k)}}^2} \right]. \tag{5.2}$$

Here, the summation of the contributions only from the neighboring protons is enough because of the factor of r^{-6}.

Dipole coupling consists of intramolecular and intermolecular interactions (Fig. 5.7). If the blends contain no microscopic demixed structures and if the difference in molecular mobility between PS and PVME is assumed, relatively immobile protons of PS and relatively mobile protons of PVME are placed close to each other. The intermolecular interaction has the contributions from the same and different constituent polymers in miscible polymer blends since PS and PVME molecules are mixed on the molecular level. The situations of the intermolecular interaction for the protons of PS and PVME are identical since it is decided exclusively by ϕ, namely the fraction of the mobile and immobile protons. The relaxation times of PS and PVME, however, differ since the intramolecular interaction is always present regardless of ϕ. This is the reason for the decomposition of the spin-spin relaxation signals into two components and the continuous change of T_2 with ϕ.

Finally, we discuss the reason the longitudinal relaxations contain only one component. It is attributable to the effect of spin diffusion as described in the following. The length between two hydrogen atoms in a CH_2 group, for example, is about 0.18 nm. Domains with the size of 1 nm and 10 nm, where spin diffusion is effective for $T_{1\rho}$ and T_1 respectively, contains at least tens of neighboring proton pairs. The difference of dipolar interactions for PS and PVME protons of model II is averaged out inside these domains.

References

[1] T. K. Kwei, T. Nishi, R. F. Roberts, Macromolecules, **7**, 667 (1974).

[2] T. Nishi, T. T. Wang, T. K. Kwei, Macromolecules, **8**, 227 (1975).

[3] V. J. McBrierty and D. C. Douglass, Phys. Rept. **63**, 61 (1980)

[4] J. S. Waugh and C. H. Wang, Phys. Rev., **162**, 209 (1967).

[5] A. Abragam, "The Principles of Nuclear Magnetism", Oxford (1961).

Acknowledgment

I would like to express my sincerest gratitude to Prof. Toshio Nishi of School of Engineering, The University of Tokyo for supervising and offering me the opportunity to research in his laboratory since my student age.

I wish to thank Prof. Reinosuke Hayakawa of School of Engineering, The University of Tokyo, Prof. Yoshiyuki Amemiya of Graduate School of Frontier Sciences, The University of Tokyo, Prof. Hajime Tanaka of Institute of Industrial Science, The University of Tokyo, Prof. Kohzo Ito of Graduate School of Frontier Sciences, The University of Tokyo, and Prof. Yasuyuki Kimura of School of Engineering, The University of Tokyo who were in charge of the present doctoral dissertation.

I am also grateful to and Prof. Takafumi Hayashi of Department of Computer Software, University of Aizu. He was Research Associate in the laboratory when I was a graduate student. Prof. H. Tanaka was in that position in my undergraduate period. I was fortunate enough to get them to give me much advice and comments on my research. I also thank to Dr. Masami Kageshima of Joint Research Center for Atom Technology, who was a technical official in the laboratory, for discussions on research.

This thesis was completed with much help from many people. I thank all of them here: Mr. Y. Nakanishi, Mr. T. Mitsui, Mr. A. Hotta, and Mr. H. Yamaguchi for the work in chapter 2, Mr. M. Shimada and Dr. Y. Nagamine for the work in chapter 3, Dr. J.-C. Lee, Mr. H. Tazawa, Ms. Y. Kosaka, and Mr. T. Tazawa for the work in chapter 4, and Mr. H. Tazawa and Mr. Y. Koike for the work in chapter 5.

Finally, I would like to express my deepest gratefulness to my parents, Kotaro and Satomi Ikehara who have always supported me in my life.